The Bortoluzzi Mud Volcano (Ionian Sea, Italy) and its potential for tracking the seismic cycle of active faults

Marco Cuffaro[1], Andrea Billi[1], Sabina Bigi[2], Alessandro Bosman[1], Cinzia G. Caruso[3], Alessia Conti[2], Andrea Corbo[3], Antonio Costanza[4], Giuseppe D'Anna[4], Carlo Doglioni[2,5], Gioacchino Fertitta[4], Luca Gasperini[6], Francesco Italiano[3], Gianluca Lazzaro[3], Marco Ligi[6], Manfredi Longo[3], Eleonora Martorelli[1], Lorenzo Petracchini[1], Patrizio Petricca[2], Alina Polonia[6], and Tiziana Sgroi[5]

[1]Istituto di Geologia Ambientale e Geoingegneria, CNR, Rome, Italy
[2]Dipartimento di Scienze della Terra, Sapienza Universitá di Roma, Rome, Italy
[3]Istituto Nazionale di Geofisica e Vulcanologia, Palermo, Italy
[4]Istituto Nazionale di Geofisica e Vulcanologia, Gibilmanna, Italy
[5]Istituto Nazionale di Geofisica e Vulcanologia, Rome, Italy
[6]Consiglio Nazionale delle Ricerche, ISMAR, Bologna, Italy

Correspondence: Andrea Billi (andrea.billi@cnr.it)

Abstract. The Ionian Sea in southern Italy is at the center of active interaction and convergence between the Eurasian and African-Adriatic plates in the Mediterranean. This area is seismically active with instrumentally/historically-recorded Mw > 7.0 earthquakes and it is affected by recently-discovered long strike-slip faults across the active Calabrian accretionary wedge. Many mud volcanoes occur on top of the wedge. A recently-discovered one (here named Bortoluzzi Mud Volcano, BMV)

5 was surveyed during the Seismofaults 2017 cruise (May 2017). Bathymetric-backscatter surveys, seismic reflection profiles, geochemical and earthquake data as well as a gravity core are here used to geologically, geochemically, and geophysically characterize this structure. The BMV is a circular feature ≃22 m high and ≃1100 m in diameter with steep slopes (up to a dip of 22°). It sits atop the Calabrian accretionary wedge and a system of flower-like oblique-slip faults that are probably seismically active as demonstrated by earthquake hypocentral and focal data. Geochemistry of water samples from the seawater column on

10 top of the BMV shows a significant contamination of the bottom waters from saline (evaporite-type) CH_4-dominated crustal-derived fluids similar to the fluids collected from a mud volcano located in the Calabria main land over the same accretionary wedge. These results attest for the occurrence of an open crustal conduit through the BMV down to at least the Messinian evaporites at about -3000 m. This evidence is also substantiated by Helium isotope ratios and by different geochemical data from three sea water columns located elsewhere in the Ionian Sea. Conclusions are drawn on the origin of the BMV and on

15 the potential of this type of structures for tracking the seismic cycle of active faults. Due to the widespread diffusion of mud volcanoes in seismically active settings, this study may contribute to indicate a potential and feasible future path for the use of these ubiquitous structures in favor of the mitigation of natural hazards.

Copyright statement. TEXT

1   Introduction

Mud volcanoes are ubiquitous structures on the Earth's surface both in marine and in continental settings and form for a variety of causes, most of which amenable to clay- and fluid-rich subsurface levels, where overpressures contribute to drive the ascent of mixed and liquefied clay, water, and gases (e.g., CO_2, CH_4, and N), with consequent formation of the conical or

5   conical-trunk landform (Milkov, 2000; Deville et al., 2003; Etiope and Milkov, 2004; Planke et al., 2003; León et al., 2007; Ceramicola et al., 2014; Sella et al., 2014). Mud volcanoes can be therefore taken as markers of overpressure-related geofluid circulation, efflux, and ascent (Bertoni and Cartwright, 2015; Kirkham et al., 2017).

Many mud volcanoes occur on active accretionary prisms (Higgins, 1974; Cita, 1981; Barber, 1981; Dimitrov, 2002; Kopf, 2002; Rabaute and Chamot-Rooke, 2007; Panieri et al., 2013; Ceramicola et al., 2014; Barnard et al., 2015), where their

10   degassing activity is at least in part connected with active compression and subsequent faulting and fracturing (Camerlenghi et al., 1995; Robertson and Kopf, 1998; Kopf, 2002; Chamot-Rooke et al., 2005; Rabaute and Chamot-Rooke, 2007; Mazzini et al., 2007, 2009; Panieri et al., 2013). It is also noteworthy that, in these active tectonic settings, the longevity of mud volcanoes may even exceed 1 Ma (Cita et al., 1989; Camerlenghi et al., 1992, 1995; Robertson, 1996; Robertson and Kopf, 1998; Kopf et al., 1998; Praeg et al., 2009; Somoza et al., 2012), and they - all together the known submarine mud volcanoes -

15   release about 27 Mt methane a^{-1} (plus other gases; Milkov et al., 2003; Etiope and Milkov, 2004).

The Ionian Sea between eastern Sicily and southern Calabria (Italy; Fig. 1) hosts an active accretionary prism (the Calabrian Arc; Minelli and Faccenna, 2010; Polonia et al., 2011, 2016; Gutscher et al., 2016), where both prism-parallel thrusts and across-prism strike- and oblique-slip faults are active (Polonia et al., 2012; Totaro et al., 2013; Doglioni et al., 2012). Some of these faults could even be the source structures of some among the most devastating earthquakes and tsunamis of southern Italy

20   and the entire Mediterranean. Among other devastating events in the Ionian Sea large area, we recall the 1908 (Mw 7.2), 1783 (Mw 6.9), 1693 (Mw 7.4), 1169 (Mw 6.6), and 362 (Mw 6.6) AD earthquakes and tsunamis, which caused damage, devastation, and death (more than 80,000 deaths in 1908) in eastern Sicily and southern Calabria (Locati et al., 2016). Although such events have been studied by many authors for the great impact they produced, their origin (zone and generation mechanism) is still heavily debated both for earthquakes and tsunamis. In other words, the faults that generated such earthquakes are not yet known

25   as it is unknown whether the associated tsunamis were generated directly by earthquakes (i.e., fault dislocation of seabed) or indirectly by seismically-triggered submarine slides (Valensise and Pantosti, 1992; Billi et al., 2008, 2010; Argnani et al., 2009; Polonia et al., 2016).

To better define the seismic behavior of active faults in the Ionian Sea, during the Seismofaults 2017 and 2018 marine surveys (May 2017 and 2018, respectively; www.seismofaults.it), we deployed eleven seabottom seismometers (OBS/H) and

30   two seabottom multiparameric geochemical-geophysical sensors. One of the aims of this project and related surveys was to contribute to the advancement of the science of earthquake forecasting. For this reason, we deployed the multiparameric sensors (i.e., to detect anomalous degassing prior to earthquakes), collected sea water column samples along and far away from (active) faults, and searched for new fluid venting structures such as mud volcanoes. We believe, in fact, that the activity of some of these latter structures may be partly connected with (seismic) faulting (Martinelli et al., 1995; Polonia et al., 2011; Capozzi

et al., 2012; Panieri et al., 2013; Ceramicola et al., 2014). Discovering and monitoring such structures may therefore be the key, in the future, to better understand the seismic cycles and possible accompanying or precursory processes and phenomena such as anomalous fluid discharge from mud volcanoes (Martinelli and Ferrari, 1991; Martinelli et al., 1995; Milkov, 2000; Dimitrov, 2002; Kopf, 2002; Mazzini and Etiope, 2017). Noteworthy examples of earthquake geochemical precursors are

5 documented in many previous works (Wakita et al., 1988; Igarashi et al., 1995; Claesson et al., 2004; Huang and Ding, 2012; Inan et al., 2012; Skelton et al., 2014; Sano et al., 2016; Barberio et al., 2017; Petitta et al., 2018) and are very promising for the science of earthquake forecasting.

Following the above-mentioned reasons and aims, during the Seismofaults 2017 scientific cruise in the Ionian Sea (Fig. 1), we surveyed a large mud volcano recently signaled on the Calabrian accretionary prism by Gutscher et al. (2017) and

10 Loher et al. (2018) but never analyzed in detail (Supplement, Movies S1 and S2). We performed a multidisciplinary analysis on this feature, including high-resolution multibeam bathymetry, high frequency chirp-sonar profiling, physical and chemical analyses of the water column above the mud volcano, and gravity coring on one side of this structure. Based on these new data integrated with previous ones, we interpret the recently-discovered mud volcano within the framework of the (seismically) active accretionary prism of Calabria and eventually provide some implications for future marine researches and monitoring of

15 the seismic cycle in marine areas. Our main aim is not only to characterize the mud volcano but also to provide a contribution toward a potential and feasible future path for the use of these ubiquitous structures in favor of the mitigation of natural hazards. As the mud volcano studied in this paper had already been observed years ago by our colleague Giovanni Bortoluzzi in one of his numerous marine surveys, we name this structure the Bortoluzzi Mud Volcano (BMV) to recall his memory and fruitful life spent sailing for the science over the Mediterranean Sea and the oceans.

2 Geological Setting

The BMV is located on top of the Calabrian Arc (Ionian Sea; Fig. 1) that has developed along the Africa-Eurasia plate boundary in the center of the Mediterranean Sea. The arc belongs to the eastward retreating Apennines subduction system connecting the NW-SE-trending Apennines with the E-W-oriented Maghrebian thrust-fold belt (Patacca and Scandone, 2004). In particular, the Calabrian Arc has developed on top of a NW-dipping subduction system with the Ionian lithosphere sinking

25 toward NW beneath the Tyrrhenian lithosphere. This subduction system is also characterized by an active volcanic arc (the Aeolian Islands in the southeastern Tyrrhenian) and a well-defined Wadati–Benioff zone (Wortel and Spakman, 2000), with earthquakes descending to nearly 500 km depth beneath the Aeolian Islands on the Tyrrhenian lithosphere. The Africa-Eurasia convergence is active in this area at a very slow rate (5 mm/yr or even less), as documented by recent GPS studies (Serpelloni et al., 2007; Billi et al., 2011; Palano et al., 2012, 2015). The external part of the Arc is represented by a 300 km wide accre-

30 tionary complex bounded to the south by the outer deformation front and laterally by two major structural discontinuities: the Malta escarpment to the southwest and the Apulia escarpment to the northeast. To the northwest (i.e., toward the Calabria region), the accretionary wedge is significantly thickened (Cernobori et al., 1996), whereas it tapers away toward the southeast in the Mediterranean Sea. The wedge is segmented along strike in different structural domains by NW-trending structural disconti-

nuities. The compartments are characterized by different rheologies and deformation styles (Polonia et al., 2011). In particular, three main morpho-structural domains can be identified in the subduction complex: (i) the post-Messinian accretionary wedge; (ii) the pre-Messinian accretionary wedge, and (iii) the inner plateau. Structural styles and seafloor morphologies vary in these four compartments in correlation with different tectonic processes that include frontal accretion, out-of-sequence thrusting,
5 underplating, and complex faulting.

In the Calabrian Arc, the very low tapered (taper angle about 1.5°) outermost accretionary wedge is a salt-bearing complex developed during and after the Messinian salinity crisis (Fig. 1). Frontal accretion of the arc is active in this southern region over a shallow basal detachment located within or at the base of the Messinian evaporites. The inner wedge, which is located toward NW at the rear of the post-Messinian accretionary complex, consists of pre-Messinian clastic sediments. The basal thrust of the
10 inner wedge is located on top of the Cretaceous sediments and/or at the transition with the basement. Moreover, the inner wedge is bounded toward NW by an inner deformation front, representing the transition between the strongly deformed accretionary wedge to the SE and a less deformed inner plateau to the NW. This plateau is however dissected by long normal and strike-slip fault zones mostly striking NW-SE. The inner plateau is characterized by chaotic units (Rossi and Sartori, 1981) and many mud volcanoes (Praeg et al., 2009; Ceramicola et al., 2014; Gutscher et al., 2017; Loher et al., 2018) including the BMV that
15 is studied in this work.

As mentioned above, the Calabrian accretionary wedge is cut across (NW-SE) by a set of long faults or deformation zones (Fig. 1). Most of these tectonic features are active and characterized by strike-slip to transtensional or transpressional (oblique) kinematics. At a broad scale, the sense of horizontal shear along these zone is usually right-lateral (Argnani and Bonazzi, 2005; Minelli and Faccenna, 2010; Polonia et al., 2011, 2016, 2017; Gallais et al., 2012, 2013; Gutscher et al., 2016; Bortoluzzi et al.,
20 2017). Below, we show that the BMV is located on top of one of these oblique-slip features crossing the Calabrian accretionary wedge.

3 Methods and Results

3.1 Rationale

The main target of this work is the BMV located at 37° 53' 01" N and 16° 16' 50" E in the Ionian Sea (Fig. 1). During
25 the Seismofaults 2017 cruise, in the BMV area, we acquired high-resolution multibeam bathymetry (bathymetry, backscatter and water column), chirp seismic profiles, physical and geochemical data of the sea water column, and a sediment gravity core. These data are described below together with a re-processed and unpublished seismic reflection profile whose track is only about 200 m far away from the BMV. We integrated the above-mentioned geological-geophysical-geochemical evidence with previously-published data and with data from public databases (e.g., earthquake data). All these data are presented in
30 the next sub-sections, where the description of each type of data and results is anticipated by a synthetic description of the acquisition and processing methods together with an account of the data source. Some data (i.e., the single- and multi-channels seismic reflection profiles as well as the gravity core) are also briefly interpreted to make the subsequent discussion section easier to read and understand. The discussion section is indeed devoted to a synthesis of results and to issues more general

than the interpretation of the single dataset. All used data are reported in the figures and tables of this paper and related supplementary material. Moreover, with this paper, we release 4970 km^2 of newly-acquired (during the Seismofaults 2017 cruise) high-resolution bathymetric data in the Ionian Sea including the BMV area (Fig. S1).

3.2 Earthquakes

3.2.1 Method and Data

To understand whether the study area (BMV) is seismically active, we collected earthquake data from a public database and from previous articles. In particular, we collected crustal (depth ≤ 40 km) earthquake hypocentral-epicentral data (Table S1) from the public database of INGV Centro Nazionale Terremoti (http://cnt.rm.ingv.it/) relocated in this study by one of us (T.S.). Moreover, to understand the kinematics of the seismic faulting, we collected earthquake focal mechanisms (Table S2) from the European-Mediterranean Regional Centroid-Moment Tensors (RCMT) catalog (http://rcmt2.bo.ingv.it/) and from previous papers by Orecchio et al. (2014) and Polonia et al. (2016). Earthquake data (Tables S1 and S2) are shown in map view in Figs. 1 and 2(a) and in vertical cross-sectional view in Fig. 2(b).

3.2.2 Results

Earthquake epicenters and focal mechanisms (Figs. 1 and 2) show that the area surrounding the BMV is seismically active as it is populated by earthquakes. In particular, the earthquakes recorded in the BMV area between 1985 and 2017 at depths ≤ 40 km are 178 (Mw ≤ 4.4; Table S1). Focal mechanisms are from earthquakes that are ≤ 4.5 in magnitude and ≤ 30 km in depth (Table S2). Focal mechanisms are mostly characterized by strike-slip and transtensional faulting along NW-SE-striking planes or along the conjugate planes striking NE-SW. Fig. 2(b) shows a transect-perpendicular projection of the above-described earthquake data (i.e., hypocenters; Tables S1 and S2) along a NE-SW vertical transect through the BMV (see the A-A' transect track in Fig. 2a). Projected seismic events were selected within a distance of 12 km from the transect track (Fig. 2a). The cross-sectional view of Fig. 2(b) shows that earthquake hypocenters are diffuse over the studied transect including the area beneath the BMV. A cluster of hypocenters is discernible near the northeastern tip of the transect (Fig. 2b). This same cluster is also visible as a NW-trending cluster of epicenters in the northeastern portion of the study area (i.e., 40 km to the northeast of the BMV; Fig. 2a).

3.3 Bathymetry and Geomorphology

3.3.1 Method and Data

We carried out the high resolution multibeam bathymetric survey (Fig. S1) using a multibeam Teledyne Reson SeaBat 7160 (41-47 kHz) echosounder characterized by footprint size of 1°× 1°. We identified precise positioning through differential GPS (accuracy ±0.5 m), while we derived sound velocity profiles from multiple Conductivity-Temperature-Depth (CTD) casts (Seabird 911plus) to ray trace the acoustic wave along the water column. We processed multibeam data on board using Caris

Hips & Sips hydrographic software with the following parameters and processing methods: (a) corrections for tidal height variations from the Catania harbor tide gauge (www.mareografico.it); (b) multibeam calibration (patch test) to measure the angular misalignment between the transducers, motion sensor, gyro, and the position latency; (c) statistical and geometrical (angle and distance) filters to remove coherent and incoherent noise in each swath; (d) manual removal of isolated fake soundings; and

5   (e) generation of a high resolution digital marine model, with a resolution varying between 10 m in deep water (down to -1000 m water depth) and 25 m at greater depths (Bosman et al., 2015). In particular, we calibrated the multibeam data through a patch test in an area located at 1600 m water depth close to a morphological high and a sub-linear slope. The multibeam patch test conducted with PDS2000 and verified with Caris H&S provided the following values: Time delay: 0.0; Heading correction: -0.930°; Roll correction: 0.680°; and Pitch correction: -1.020°. We used backscatter images and observations of raw data

10   scattering along the water column to verify anomalies of amplitude on the seafloor and along the water column. However, compatibly with the instrumental resolution and the depths of the BMV, the data did not show any significant anomaly of the amplitude of the signals or significant evidence of fluid escape.

3.3.2 Results

The study area is located on the upper part of the continental slope of the Calabrian-Ionian margin (Figs. 1 and S1) between

15   120 m and 2000 m water depth. This area is characterized by a complex morphology due to the interaction between tectonically controlled escarpments and several small scale mass-wasting features, including landslide scars and gullies/channels (Fig. 3). The upper part of the continental slope is characterized by a very steep slope (about 15°) that reaches a maximum of 22° or, in places, even 28°, along the main escarpments oriented NE-SW and long up to 35 km (Fig. 3b). At the foot of the upper continental slope, a well-defined flat area of about 26 km^2 occurs encompassing the sub-circular morphological high of the

20   BMV (Fig. 3). The flat area is located at 1350 m water depth and bordered by several small ridges that are elongated parallel to the continental slope. The BMV is characterized by a circular shape with a diameter of about 1100 m and a well-defined rim (Figs. 3 and 4). The BMV has an elevation of about 22 m from its base (i.e., the surrounding plain) and steep slopes dipping up to 22° (see the slope profile in Fig. 4a). The high resolution digital elevation model shows some complex structural and morphological features (Fig. 4). These features consist of concentric morphologies with a perimetric topographic rim, separated

25   by some moats and encompassed by the outermost topographic rim of the BMV (Fig. 4). Furthermore, on top of the BMV, three minor sub-circular/arcuate bulges are present. These features have a relief of about 3 m with respect to the surrounding seafloor and are separated by small sub-circular moats (Fig. 4b). The outermost topographic rim of the BMV is interrupted in the southern side (Fig. 4b). Low resolution backscatter data indicate low amplitude of acoustic signals whereas the absence of changes/anomalies in the amplitude indicates a clayey/pelitic sedimentary cover (Fig. 5a). In addition, consistently with the

30   resolution of the multibeam equipment, multibeam water column data recorded during the Seismofaults 2017 survey does not highlight acoustic backscatter anomalies related to large amount of fluids escaped from the seafloor (Fig. 5b; e.g., Römer et al., 2014).

To better understand the morphology of the BMV, also in comparison with other known mud volcanoes on the Earth, we here consider recent compilations of mud volcano morphological data (e.g., Kioka and Ashi, 2015; Kioka et al., 2015). We

refer, in particular, to the works by Kirkham et al. (2017) and Kioka and Ashi (2015), where relations between mud volcano height H vs. diameter D, and volume V vs. H/R ratio (where R is the radius of the volcano base) are explored, respectively. We used the mud volcano dataset reported by Kioka and Ashi (2015), selecting 232 mud volcanoes with available mean diameter D and height H (Fig. 6a). Fig. 6 shows H vs. D (Figs. 6b and 6c) and V vs. H/R (Fig. 6d) for the 232 selected mud volcanoes.

5   Volumes are calculated following the method proposed by Kioka and Ashi (2015), i.e., using the relation $V = \pi R^2 H/3$, that is the volume of the cone even though many volcanoes have a flat-topped summit and may be better approximated to a trunk cone (e.g., the BMV). Figs. 6(b and c) shows that some mud volcanoes display a large diameter but low relief, whereas very few mud volcanoes exhibit small diameter but prominent topography. An approximately linear trend between increasing diameters and heights can be inferred. In this trend, the BMV stands close to the lower D and H values. Fig. 6(d) shows that the H/R ratio

10 of all mud volcanoes is ≤0.4. The same ratio for the BMV is < 0.1. There is a scattered distribution of volumes (V), mostly ranging in the 106-109 m^3 interval. The BMV volume corresponds to 6.9 x 106 m^3 (Fig. 6d).

3.4   Single-channel Chirp Seismic Reflection Profiles

3.4.1   Method and Data

During the Seismofaults 2017 survey, to define the local geological setting and a high resolution seismic stratigraphy of the

15 BMV and surrounding area, we acquired a set of chirp seismic profiles (Figs. 7b-d, 8, and S2) using a frequency-modulated source operating in the frequency range of 2-7 kHz (Benthos Chirp III) and recorded with a 0.5-0.8 s sweep length. Maximum sub-bottom penetration is up to about 40 ms (TWT) and vertical resolution is about 0.7 ms (TWT). We processed the chirp profiles using the GeoSuite All Works software, applying Time Varied Gain. Thicknesses and depths of seismic profiles are described in two-way travel time (TWT; Figs. 7b-d and 8), with a seismic velocity of 1500 m/s being used to convert two-way

20 travel time into depth. Seismic data interpretation was carried out through the Kingdom Suite software also integrating the bathymetric data and a gravity core (Fig. 9).

3.4.2   Results

In the chirp seismic profiles (253, 241, and 246 in Fig. 7b-d), we recognized the following seismostratigraphic units:

Unit U0 corresponds to the seafloor seismic unit of the BMV and is characterized by sharp bottom echoes with no sub-

25 bottom reflections or little acoustic penetration with chaotic reflections and locally large hyperbolae. Adjacent to the BMV, we recognized the following four further seismic units (U1, U2, U3, and U4).

Unit U1 is mostly characterized by parallel to subparallel semi-continuous reflections with variable amplitude. The upper boundary (H1) is locally erosive in the sector adjacent to the BMV and tends to become a conformity surface far away from the BMV. Locally, toward the northern escarpment, reflections in U1 are truncated by an erosional surface. Adjacent to the BMV,

30 normal faults displaced this unit.

Unit U2 is characterized by a quasi-transparent (reflection free) seismic facies and shows draping of the underlying relief. This unit has a wedge-shaped morphology, thickening toward the flank of the BMV (241 in Fig. 7c), where it reaches a

thickness of at least 25 ms. The lower boundary of U2 is the horizon H1, whereas the upper boundary is an erosional surface (H2) with local extent. U2 is distributed in the sector comprised between the northern escarpment and the BMV and is confined by the northern escarpment. Locally, U2 can be recognized also along the southern flank of the BMV edifice (246 in Fig. 7d).

Unit U3 is characterized by high amplitude reflections and by a limited thickness. The internal filling configuration of this

5   unit is a parallel onlap. Locally, the seismic facies is semitransparent. The lower boundary of U3 is represented by horizon H2 whereas the upper boundary is horizon H3 that is locally characterized by erosion.

Unit U4 is characterized by a transparent/chaotic seismic facies (241, 246, and 253 in Fig. 7b-d). It has a wedge-shaped morphology and thickening toward the northern escarpment (max. thickness of about 20 ms). The lower boundary of U4 is represented by horizon H3, locally characterized by erosion. The upper boundary is the seafloor. U4 is well discernible (max.

10   thickenss = c. 20 ms TWT) in the sector comprised between the northern escarpment and the BMV and less discernible but still present (max. thickenss = c. 4 ms TWT) to the south of the BMV.

Based on the seismic characters, we interpret the five seismic units as follows (Fig. 8):

Unit U0 is interpreted as the BMV main edifice. The transition between the rim and the summit caldera is identified by the large hyperbolae. The floor of the summit caldera is not penetrated by seismic signal, possibly indicating the occurrence of

15   mud breccias deposits that are typical of mud volcanoes (van der Meer, 1996; Gennari et al., 2013).

Unit U1 is interpreted as slope deposits including turbidite-hemipelagite intervals. Locally, slope deposits are eroded by U2 (i.e., mud volcano deposits).

Unit U2 is interpreted as a mud volcano deposit belonging to the BMV, due to its wedge-shaped quasi-transparent (reflection free) seismic facies thinning away from the BMV center. This deposit can be related to eruptive events or post eruptive

20   instability of the following types:

(1) Buried mudflow deposits: gravity flow deposits related to slope instability of the mud volcano.

(2) Buried mud volcano sediment: similar wedge-shaped seismic units have been interpreted by Evans et al. (2008) as massive and structureless sediment extruded from the volcano center (see, for comparison, figures 7 and 8 in Evans et al., 2008).

25   Unit U3 is interpreted as ponded deposits, including turbidite-hemipelagite intervals and thin mass transport deposits. Locally, ponded deposits are eroded by U4 (i.e., mass transport deposits).

Unit U4 is interpreted as consisting of mass transport deposits originated by slope instability along the northern escarpment (i.e., toward the coast). This interpretation is based on the quasi-transparent (reflection free) seismic facies of this unit and on its wedge shape with reduced thickness moving away from the northern escarpment. Interpretation of U4 is also based on

30   direct evidence from the gravity core of Fig. 9 (see next subsection).

3.5 Seabottom Gravity Core

3.5.1 Method and Data

We collected the SF17-01 core using a 1.2 ton gravity corer with coring pipes 6 m long (see location in Fig. 7a). We analyzed the core sections through a multi-proxy approach involving high-resolution digital photographs and determination of physical

5 properties and sand content as deduced through the weight of selected samples. We also acquired high resolution magnetic susceptibility (MS) through a core log system (Bartinghton model MS2, 100 mm loop sensor) with a sampling interval of 1.0 cm.

3.5.2 results

We collected the SF17-01 core at the toe of the peripheral rim marking the external slopes of the BMV (Fig. 7a). Chirp

10 profiles collected during coring operations (Figs. 7b-d and 8) shows a chaotic unit (U4, Figs. 7b-d and 8) resting on the mud volcano flanks possibly related to re-sedimentation processes (e.g., slumping or turbidity currents). Chirp-core correlation suggests that the chaotic and transparent sediments are represented by the 2-m-thick fining-upward resedimented unit between 0.50 and 2.50 m depth (Fig. 9). The base of this unit is marked by an abrupt increase in sand content and by an erosional basal contact (Fig. 9).

15 Although the gravity core did not sample mud breccias, it shows indirect evidence of fluid/mud flow as pointed out by the presence of patchy/cloudy facies where sediment disturbance is caused by fluid expulsion. The sampled section below the base of the resedimented unit is characterized by silty-clay bulk sediments containing irregularly clustered intervals of differently colored sediment patches (from dark grey, olive grey and brownish clouds within grey matrix) with several fragmented and vertically dislocated thin silty turbidites and volcanoclastic layers (Fig. 9). Sediments contain several vertical or sub-vertical

20 micro-pipes suggesting sediment reworking by fluid migration. We associate this sediment structure to the patchy/cloudy facies (e.g., Staffini et al., 1993; Cita et al., 1996), which was already described in the surrounding areas in association with mud volcanism (Panieri et al., 2013). The presence of the patchy/cloudy facies in the core is identified by changes in magnetic susceptibility, whereas the sand content does not show diagnostic changes (Fig. 9).

3.6 Multi-Channel Seismic Reflection Profiles

25 #### 3.6.1 Method and Data

In this section, we present two multiple channel seismic reflection profiles and related interpretations (Fig. 10; see tracks in Fig. 1). The first profile (Fig. 10a) is the CROP M-31 (Scrocca et al., 2003) in the version interpreted by Polonia et al. (2016). The second profile is the CA99-215 (Fig. 10b) both in the version interpreted by Polonia et al. (2016) and in a new version (Figs. 10c and 10d; see also Fig. S2) deriving from a recent reprocessing kindly provided by Spectrum Geo Ltd

30 (http://www.spectrumgeo.com/) within the framework of a confidentiality agreement between Spectrum Geo and Sapienza University of Rome. The CA99-215 profile was acquired in 1999 and reprocessed in 2001. Reprocessing mainly consisted

in a standard PSTM (pre-stack time migration) processing sequence, resulted in an improved data quality. Stratigraphic syntheses from the Fosca 1 and Floriana 1 wells (original well data are from the Videpi public database available online at http://unmig.sviluppoeconomico.gov.it/videpi/videpi.asp) are also presented (Fig. 10f) to help interpreting the seismic profiles (see well location in Fig. 1).

3.6.2 results

The CROP M-31 and CA99-215 profiles (Fig. 10) are located within the inner plateau of the Calabrian Arc, a morphologically flat area with forearc basins formed on the top of the continental basement (Polonia et al., 2011, 2016). The inner plateau of the Calabrian Arc is characterized by a generally thick portion of Plio-Quaternary deposits overlying the Messinian sediments sampled in several nearby boreholes (e.g., Floriana 1 and Fosca 1 wells; Figs. 1 and 10f) and recognized both in the CROP M-31 and in the CA99-215 seismic profiles (Polonia et al., 2016). Below the Messinian deposits, the upper Oligocene-upper Miocene turbidite deposits unconformably overlie the basement units.

The seismic profiles are characterized by different structural domains with peculiar deformation patterns (Polonia et al., 2016). In particular, the Ionian Fault system (see this system in map view in Fig. 1) is observed in the seismic profiles (between s.p. 1100 and 1400 of the CROP M-31 profile and on the western side of the CA99-215 profile). The Ionian Fault system, characterized by transtensive faulting, seems to re-activate pre-existing Miocene-Pliocene thrusts (Polonia et al., 2016) and it separates the Calabrian Arc into two sectors: the Western and the Eastern lobes (Figs. 1 and 10).

The Eastern Lobe, where the BMV is located, is characterized by a more elevated accretionary wedge and by steeper topographic slopes than those of the Western Lobe, as shown in the sector between s.p. 1500 and 2600 of the CA99-215 profile (Fig. 10; Polonia et al., 2011).

The CA99-215 profile displays numerous faults characterized by different kinematics and related to the complex evolution of the area, namely: thrust faults, which are the result of the post-Messinian shortening, and normal faults deriving from the extensional process acting in more recent times (from lower Pleistocene to present times) as shown by the faults reaching the sea bottom on the eastern side of the seismic profiles (Fig. 10). Earthquakes focal mechanisms located in the study area (Figs. 1 and 2) show that faults are mostly characterized by strike-slip and transtensional kinematics defining a flower-like oblique-slip deformation zone (Fig. 10b). In this area, one of the main reflective horizons, usually discernible in most seismic profiles, is the top of the Messinian deposits. The Messinian deposits cored in the nearby wells (in particular in the Squillace Gulf) consist of clay-dominated deposits with interbedded gypsum, anhydrite, and halite (Capozzi et al., 2012). The Floriana 1 well shows, for instance, a thick portion (more than 1300 m) of the Gessoso Solfifera Formation (consisting of crystalline gypsum, anhydrite, and clay layers) whereas, in the Fosca 1 well, the Messinian deposits are mostly formed by clay and silt for a total thickness of 110 m (Fig. 10f). The distribution and sedimentary pattern of the Messinian deposits suggest indeed that the basin was already articulated and tectonically controlled at the time of Messinian sedimentation (Capozzi et al., 2012). The occurrence of Messinian evaporites as well as clays and silts of the same age is very relevant for mud volcanism. Indeed, according to many studies on mud volcanoes in the Ionian Sea and in the adjacent Mediterranean Ridge (located off southern Peloponnesus and

Crete), the disruption of the Messinian low-permeability layers concurred to or was the key process controlling the ascent of pressurized fluids entrapped below these sealing layers and the consequent outflow and mud volcanism (Capozzi et al., 2012).

Zooming into the BMV area (Figs. 10d, 10e, and S2), we observe the following main features: (1) the presence of top Messinian deposits reflectors; (2) the disruption of these reflectors; (3) the presence of normal faults; and (4) the presence of

5 an area of fluid-rock interaction similar to many ones observed in seismic profiles below mud volcanoes (Capozzi et al., 2012). In particular, the area just below the BMV, which is about 200 m far away from the CA99-215 profile (Fig. 1), shows (at a time-depth of 2 s TWT) a rock volume characterized by a chaotic and slightly transparent seismic reflection signal (Figs. 10d, 10e and S2). It is relevant to note that this area is located right at the top of a series of faults. The Messinian evaporites are located between 2 and 3 s TWT. Considering a seismic velocity of 1500 m/s for the sea water column and 2000 m/s for the

10 post-Messinian column of sediments (Gallais et al., 2012), the Messinian evaporites should occur at about -3000 m.

3.7   Geochemical Features of Four Sea Water Columns

3.7.1   Method and Data

We sampled sea water columns at various depths in four localities of the Ionian Sea (Fig. 1 and Tables 1 and 2): namely, above the BMV and above the GeoC1, GeoC2, and GeoC3 localities that are along or nearby major presumably-active fault

15 zones (Polonia et al., 2012, 2016). We carried out vertical casts by Rosette and Niskin bottles to determine the geochemical features and dissolved gases at the sea bottom and along the water columns (Fig. 11 and Tables 1 and 2). Samples are compared with the local air-saturated sea water (ASSW) used as benchmark.

The samples, specifically collected for the extraction of the whole gas phase for chemical and isotopic analyses, were stored in 240 ml pyrex bottles sealed on board using rubber/teflon septa and purpose-built pliers, and analyzed within two

20 weeks. Details of the sampling methodology are reported in Italiano et al. (2009, 2014). During the cruise, the sampled bottles were stored upside down, keeping the necks with the rubber septa submerged in sea-water until they were transferred to the laboratory. The collected sea-water samples underwent laboratory procedures for both chemical (concentration of dissolved gas species) and isotopic (helium isotopes) determinations. In the laboratory, the dissolved gases were extracted after equilibrium was reached at constant temperature with a host-gas (high-purity argon) injected in the sample bottle (see Italiano et al., 2009,

25 2014, for further details). The chemical analyses of O_2, N_2, CH_4, and CO_2 were carried out by gas-chromatography (Agylent 7800B equipped with a double TCD-FID detector) using argon as carrier gas. Typical analytical uncertainties were within $\pm 5\%$. He concentration was determined by mass spectrometry, during 3He/4He analyses. Helium isotope and 4He/20Ne ratios were carried out on gas fractions extracted following the same procedure described above and purified following the method described in the literature (Hilton, 1996; Sano and Wakita, 1988; Italiano et al., 2001). The isotopic analyses of the purified

30 helium were performed using a static vacuum mass spectrometer (GVI5400TFT) that allows the simultaneous detection of 3He and 4He ion beams, thereby keeping the 3He/4He error of measurement very low. The used analytical method also requires to alternatively run one sample and one purified air shot used as internal 3He/4He standard. Typical uncertainties in the range of

atmospheric He-type samples are within $\pm 1\%$. The 4He/20Ne ratios were calculated by the relative peak heights measured on the same mass spectrometer.

Water samples of 100 ml were stored in PVC bottles for total alkalinity titration: 50 ml were filtered by a 0.45 μm filter and acidified by HNO_3 0.1 N for cations (Ca, Mg, Na, and K) determination, whereas the non-acidified samples were collected

5   for anions (Cl, F, and SO_4) determination. pH was measured by an electronic device calibrated in situ using buffer solutions. In the laboratory, chemical analyses of the major constituents were carried out by ion-chromatography (Dionex ICS-1100) both on filtered (0.45 mm) acidified (HNO_3 Suprapur) water samples (Na, K, Mg, and Ca), as well as on untreated samples (F, Cl, Br, NO_3, and SO_4). The HCO_3 content was measured by standard titration procedures with hydrochloric acid. Typical uncertainties are $\pm 5\%$.

10 **3.7.2   Results**

The analytical results in terms of chemical and isotopic composition of the water samples and the dissolved gases are listed in Tables 1 and 2, respectively. The fault zone data (GeoC1, 2, and 3) are from samples coming from vertical casts performed far from the BMV over the Ionian and Alfeo-Etna fault systems (Fig. 1). The typical composition of an Air Saturated Sea Water (ASSW) is reported for comparison (Tables 1 and 2).

15 The five sea-water samples collected along the water column over the BMV (except the sample collected near the seabed) show a chemical composition similar to the fault zone samples (GeoC1, 2, and 3; Fig. 11 and Tables 1 and 2). Although the concentration values for major cations (Na, K, Mg, Ca; Table 1) show comparable values for the GeoC1, 2, and 3 samples and the ones from the BMV (including water column and bottom samples), the Br content display small but detectable differences between the GeoC1, 2, and 3 and the BMV samples, respectively (Table 1). Along the BMV water column, the Br content

20 is between 11 and 47% higher than the GeoC1, 2, and 3 samples. Contrastingly, the dissolved gases detected along the water column (Table 2) exhibit geochemical features with large differences from the sea water equilibrated with the atmosphere (ASSW). In particular, the composition of the dissolved gases (Table 2) shows the presence of air-derived gases (N_2 and O_2) along with non-atmospheric gases (CO_2 and CH_4). The analytical results clearly display a slight decrease in oxygen content (as expected) besides a significant increase in He, CH_4, and CO_2. The CH_4 content along the water column and at the sea

25 bottom (BMV and GeoC1, 2, and 3) ranges from two to three orders of magnitude higher than the ASSW with the highest concentration recorded at the BMV depth (-1337 m). The CO_2 content above the BMV, in particular, is the double of the ASSW (0.24 ccSTP/L) at the depth of 100 m and it increases up to 0.71 ccSTP/L at the sea bottom (-1337 m) (Fig. 11 and Table 1).

A few years ago (2003), one of us (FI) collected and analyzed fluid samples from a shallow well located in the Calabria main land nearby the Palizzi mud volcano (PMV in Fig. 1, located about 25 km to the WNW of the BMV area). Unfortunately,

30 no documentation exists concerning the PMV except our original geochemical data reported in Tables 1 and 2. The PMV was indeed actively venting geofluids at the time of our sampling (2003) but it was then soon destroyed by human activity and cementation. The PMV is characterized by a dissolved gas phase mainly composed by Nitrogen and CH_4 with a significant helium concentration and a slight amount of CO_2. Oxygen is below the detection limits (Tables 1 and 2).

The helium isotopic signature of samples coming from the GeoC1, 2, and 3 casts show an atmospheric signature from the surface to the depth of 1000 m. The bottom sample displays a lower ratio than the air with a higher 4He/20Ne ratio. Two samples from the BMV cast were analyzed to determine the helium isotopes. Results approximately match those from the GeoC1, 2, and 3 casts showing a slight but detectable difference with the respect to the atmospheric ratios (as expected for an ASSW) for both 3He/4He and 4He/20Ne ratios (Fig. 11 and Tables 1 and 2).

4 Discussion and conclusions

4.1 Focuses

We focus our discussion on two main aspects of the BMV, that are: (1) its origin and activity, and (2) the potential for the use of this structure and similar ones in favor of the mitigation of natural hazards.

4.2 Origin and Activity

4.2.1 General Context

Concerning the origin of the BMV, we here reconsider all the above-described data. First of all, we mention the fact that the Ionian Sea, where two active accretionary prisms occur and obliquely-converge (i.e., the Calabrian Arc and the Mediterranean Ridge), is a region rich of active or recently-active mud volcanoes (Cita, 1981; Camerlenghi et al., 1992; Limonov et al., 1996; Capraro et al., 2006; Serpelloni et al., 2007; Praeg et al., 2009; Billi et al., 2011). The BMV itself was previously signaled and hypothesized as a mud volcano by Gutscher et al. (2017) and Loher et al. (2018). The BMV occur on top of the Calabrian accretionary wedge in a rather isolated location with several further mud volcanoes occurring a few kilometers or a few tens of kilometers toward NE along the prism (Fig. 1; Loher et al., 2018).

4.2.2 Morphology

From a morphological point of view, the shape of the BMV is that typical of most mud volcanoes (i.e., pie-type, Kioka and Ashi, 2015; Kioka et al., 2015) and all its measured parameters (height, diameter, and volume; Fig. 6) are well within the range typical of marine mud volcanoes (Kioka and Ashi, 2015; Kioka et al., 2015; Kirkham et al., 2017). The stratigraphic analyses realized through direct and indirect methods (Figs. 7-10) show the occurrence of lithological units consistent with the activity of a mud volcano, such as the U2 deposits in Figs. 7c and 8, the evidence of fluid/mud flow in the patchy/cloudy facies of the gravity core (Fig. 9), and the semitransparent seismic facies (typical of mud volcanoes for the host rock-geofluid interaction; e.g., Capozzi et al., 2012) beneath the BMV (Figs. 10d).

4.2.3 Sealing

Moreover, particularly in the Mediterranean Sea, the origin of most mud volcanoes has been linked in a cause-effect relationship with the sealing action exerted by the Messinian evaporites, causing fluid entrapment underneath and consequent fluid

overpressure (Camerlenghi et al., 1995; Chamot-Rooke et al., 2005; Rabaute and Chamot-Rooke, 2007; Camerlenghi and Pini, 2009; Capozzi et al., 2012; Ceramicola et al., 2014; Rovere et al., 2014; Bertoni and Cartwright, 2015). Also in the case of the BMV, the seismic cross-sections show the presence (and disruption underneath the BMV of the Messinian evaporites (Fig. 10), which therefore may have been decisive in building the necessary overpressure of fluids to consequently form the mud

5   volcano itself. The disruption of the Messinian layers suggests that the conduit for the ascent of geofluids through the BMV is presently open. This hypothesis is also substantiated by the geochemical data (Fig. 11) that are discussed below.

4.2.4   Ongoing Activity

We have very little evidence to discuss the ongoing activity of the BMV also because we collected data from this structure only in a single campaign in May 2017. From a morphological point of view, the BMV seems well structured (Fig. 4) and

10 therefore its main edifice-building paroxysmal activity may have substantially ceased. Moreover, the flanks of the main volcanic edifice seems partly covered by younger products (i.e., over its flanks; Figs. 7c-d and 8) deriving from nearby gravity instabilities (i.e., from the continental slope of the Calabrian-Ionian margin; Figs. 1 and S1). Also, the backscatter data show no extensive anomalies (in May 2017) related to large amount of mud and fluids escaped from the seafloor (e.g., Römer et al., 2014); however, this evidence does not detract from the fact that the volcano may currently be quiescent and therefore may

15 erupt in the future. To this end, both the geochemical and the reflection seismic evidence show that some fluid activity below the BMV is probably ongoing. Fig. 11, in particular, shows a trend of CH_4 and CO_2 enrichment for all the collected samples with respect of a sea water simply equilibrated with the atmosphere (ASSW). Although CO_2 and CH_4 may derive from degradation processes of organic matter, the geochemical composition of the sea water at the BMV depth and the composition of the geofluids from the PMV (Palizzi) onland area clearly indicate a CH_4 injection that is typical of most mud volcanoes. The

20 isotopic composition of helium, although dominated by a typical atmospheric signature both at the GeoC1, 2, and 3 localities and at the BMV locality, displays a detectable increase of radiogenic 4He of typical crustal origin, with the associated decrease of the isotopic ratio from about 0.93-1 Ra to 0.77 Ra detected in the GeoC1, 2 and 3 seabottom waters and 0,73Ra in the BMV seabottom water (Tables 1 and 2). Combining the above-mentioned results with the enhanced Br content detected over the same site, we propose that the BMV has actually an open conduit as shown by the release of fluids into the surrounding sea

25 water (Fig. 11 and Tables 1 and 2). Fluids are composed by a two-phase system: a CH_4-dominated gas phase and hypersaline waters of evaporate type. The hypersaline waters are indeed probably generated by the dissolution of anciently buried evaporites (Messinian) and create dense anoxic brines with enhanced Br content, that are separated from the overlying oxygenated deep-seawater column due to their density. The semitransparent seismic facies (typical of active mud volcanoes; e.g., Capozzi et al., 2012) recorded beneath the BMV (Fig. 10) as well as the disruption of the Messinian evaporate layers supports the

30 above-proposed hypothesis of an open conduit down to the Messinian evaporate layers (c. 3000 m depth; Fig. 10). Also the gravity core bears evidence of recent fluid circulation (Fig. 9). Moreover, some structures on top of the BMV (i.e., the rim and some small ridges; Fig. 4a-b) are morphologically similar to structures related to extrusion activity of mud volcanoes (e.g., Evans et al., 2008) and are therefore probably connected with the eruptive processes and are not substantially covered by young sediments, hence attesting for a recent but undetermined time for the eruptive process of the BMV.

4.2.5 Draining Processes

In accretionary prisms, the causes (i.e., the engine) of mud volcanoes and related fluid activity are often found or hypothesized to be either the prism contraction and related fluid squeezing or the fault activity and related fluid ascent along fault damage zones. In other words, mud volcanoes can be caused by a contraction-related local dewatering or by a deeper crustal draining driven by the activity of normal and strike-slip faults (Rabaute and Chamot-Rooke, 2007; Gamberi and Rovere, 2010; Capozzi et al., 2012; Panieri et al., 2013; Ceramicola et al., 2014; Rovere et al., 2014). In the case of the BMV, we cannot unambiguously discriminate between these two main engines (prism contraction vs. fault activity). We hypothesize that both engines may concur or may have concurred to originate the BMV. Overall contraction is indeed slightly active in the Calabrian accretionary prism (Serpelloni et al., 2007; Billi et al., 2011; Faccenna et al., 2014; Polonia et al., 2016) as well as fault activity, particularly along prism-across (NW-SE) strike- to oblique-slip faults (Polonia et al., 2016, 2017). It is also true, however, that the seismological and reflection seismic data show the occurrence of a seismically-active flower-like system of faults right beneath the BMV (Figs. 2 and 10). This evidence let us think that (seismic) faulting more than the prism contraction process may have played a decisive role in the origin and feeding of the BMV, thus ultimately driving the ascent of geofluids from crustal depths. To this end, Polonia et al. (2017) have recently documented that the prism-across strike-slip faults in the Ionian Sea region are active and have been even capable of exhuming or contributing to exhume serpentinite domes from the lower plate of the Ionian subduction zone up to the upper plate and the Earth's surface.

4.2.6 Synthesis

Collectively, the data presented in this paper provide evidence for the fact that the studied structure (i.e., the BMV) is actually a mud volcano, through which fault-related crustal fluid activity and circulation is ongoing, and beneath which (seismic) faulting is active.

4.3 Potential Use of the BMV in the Science of Seismic Precursors

4.3.1 Previous Useful Results

Concerning the use of the BMV and similar structures in favor of the mitigation of natural hazards we first refer the reader to a few recent studies on geochemical precursors of earthquakes. Transient hydrogeochemical anomalies are increasingly becoming commonly recorded before M≥5.0 earthquakes at distances between 20 and more than 200 km from the earthquake epicenters. To understand their relevance for earthquake forecasting, we here briefly recall a few recent instances from Italy, Iceland, India, Japan, and Turkey. The 2016 Amatrice and Norcia earthquakes (central Italy) as well as the related sequence involved significant pore pressure changes and fluid movements both at deep and shallow crustal levels (Petitta et al., 2018; Tung and Masterlark, 2018), and were anticipated by hydrogeochemical anomalies recorded since April 2016 in springs from the central Apennines. In particular, increases of As, V, and Fe contents were recorded in groundwaters from springs monitored in the Sulmona area, about 70 km to the southeast of the epicentral area. Similar anomalies (i.e., As, V, and Fe) were also

recorded in groundwaters from the San Chiodo spring located within the epicentral area (Barberio et al., 2017). In 1995, eight months before the Mw 7.2 Kobe earthquake (Japan), the Cl and SO_4 concentrations in groundwater started to significantly and anomalously increase (20-30 km from the epicenter). Nine days before the earthquake, a peak in Rn concentration was also recorded (King et al., 1995). In 2002, anomalies in Cu, Zn, Mn, and Cr concentrations were recorded in groundwater 1, 2, 5,

5 and 10 weeks, respectively, before a Mw 5.8 earthquake in northern Iceland (90 km from the epicenter; Claesson et al., 2004). In 2012, anomalous increases of Ca, Mg, K, and Cl concentrations in groundwater together with decreases of Na and SO_4 concentrations started between at least 20 and 30 days before the Mw 7.1 Van earthquake, Turkey (20 km from the epicenter; Inan et al., 2012). In 2012, significant increases in the Na, Si, and Ca concentrations were recorded in groundwater 4-6 months before two Mw≥5.5 earthquakes in northern Iceland (70-80 km from the epicenter; Skelton et al., 2014). In 2004 and 2005,

10 transient hydrogeochemical anomalies were detected in aquifer located to north of the Shillong Plateau, Assam, India, before two Mw≥5.0 earthquakes (200 km from the epicenter). The [Na+K]/Si, Na/K, and [Na+K]/Ca ratios as well as conductivity, alkalinity, and Cl concentrations began increasing 3–5 weeks before the Mw 5.3 earthquake whereas the Ba/Sr ratio began decreasing 3–6 days before the Mw 5.0 earthquake (Skelton et al., 2008). In 2017, oxygen isotopic ratio anomalies of +0.24 $^0/_{00}$ relative to the local background were recorded in groundwater a few months before the Mw 6.6 Tottori earthquake in

15 southwest Japan (5 km from the epicenter; Onda et al., 2018).

4.3.2 The BMV

The geochemistry of the sea water column (sampled in May 2017) above the BMV compared with the sea water benchmark (ASSW; Fig. 11) shows a clear mineralization of the BMV-related waters together with an injection of CO_2 and CH_4, particularly in proximity of the BMV depth (Fig. 11). Moreover, the Helium isotope ratios (Table S4) shows a contribution by

20 crustal fluids, also in this case particularly in proximity of the BMV depth. The ion content of the BMV-related waters (Table 1) is consistent with evaporite-type waters and this notion, in turn, is consistent with the hypothesis that the fluids feeding the BMV and other mud volcanoes in the Mediterranean area are entrapped below and within the Messinian evaporites (Fig. 10d; Camerlenghi et al., 1995; Chamot-Rooke et al., 2005; Capozzi et al., 2012; Ceramicola et al., 2014; Rovere et al., 2014; Bertoni and Cartwright, 2015). Below the BMV, these rocks occur at about -3000 m (Fig. 10d). The CO_2 and CH_4 (particularly

25 CH_4) high content of the BMV-related waters is consistent with most mud volcanoes around the world (Milkov, 2000; Deville et al., 2003; Etiope and Milkov, 2004). Moreover, the decreasing content of CO_2 and CH_4 moving (shallowing) from the BMV summit upward to the sea surface is a clear symptom that the source of these dissolved gases is the BMV itself. We therefore infer that, although the BMV is not likely undergoing full mud-volcanic activity (at least during our survey in May 2017; see water backscatter data in Fig. 5b) a crustal fluid conduit through this structure is open and actively venting. This hypothesis is

30 also corroborated by the comparison with the geochemistry of three sea water columns above presumably-active fault zones in the Ionian Sea (GeoC1, 2, and 3; Figs. 1 and 11). These three sea water columns are indeed characterized by a very low content of CH_4 and by a content of CO_2 significantly lower than that obtained for the sea water right on top of the BMV (i.e., at the BMV depth; Fig. 11).

4.3.3 Synthesis

Collectively, the geochemical, geophysical, and geologic data presented in this paper show that the BMV, likewise other onshore monitoring stations previously realized (e.g., Claesson et al., 2004; Skelton et al., 2014; Barberio et al., 2017; Huang et al., 2017), could be a proper site where installing a cabled submarine multiparametric station (Fig. 12) to study possible

5 relationships between the seismic cycle of the underlying active faults and geofluid emissions. Similar stations are active onshore in Italy, Iceland, China, and elsewhere, but, to the best of our knowledge, have never been installed in marine settings. In the case of the BMV and other mud volcanoes, dissolved gases such as CO_2 and CH_4 may rather easily be monitored by submarine devices (Annunziatellis et al., 2009; Roberts et al., 2017). In particular for the seismically-active Ionian Sea, many other existing mud volcanoes (Gutscher et al., 2017; Loher et al., 2018) may host a monitoring station, but the BMV is so far

10 the one characterized by the largest geological, geophysical, and geochemical dataset and its location seems connected with seismically-active faults (Fig. 2).

5 Conclusions

(1) The BMV on the Ionian Sea is, as previously hypothesized, a mud volcano.

(2) Although evidence to support an ongoing robust and paroxysmal fluid circulation through the BMV are missing, the

15 geochemistry of the water column above the BMV shows a clear contribution from crustal geofluids.

(3) This geochemical evidence support the hypothesis of a cause-effect relationship between the BMV, the underlying active faults, and crustal-scale fluid circulation.

(4) It follows that the BMV and perhaps similar structures elsewhere could be selected in the future to geochemically tracking the seismic cycle of active faults as already done elsewhere in onshore localities.

20 (5) For what concerns the study area (Ionian Sea), on a first approximation, the presented geochemical data indicate that the BMV is a structure and locality for a potential monitoring station of the seismic cycle more suitable than fault zones, where the geochemical anomalies are significantly milder.

Data availability. All data used for this paper are available in numerical and graphical forms in the tables and diagrams/images, respectively, in the paper itself or in the supplement associated to this paper. The gravity core collected from the Ionian seabottom is visible at ISMAR

25 Bologna, Italy (http://www.ismar.cnr.it/organizzazione/sedi-secondarie/bologna) through the following contacts: alina.polonia@bo.ismar.cnr.it and luca.gasperini@bo.ismar.cnr.it. With this paper, we release 4970 km^2 of newly-acquired (during the Seismofaults 2017 cruise) high-resolution bathymetric data in numerical form for the Ionian Sea including the BMV (Fig. S1).

Author contributions. All authors actively participated in conceiving the experiment and the paper, in discussing all results, in contributing to the writing of the paper and to the drawing of all figures, and in drawing the conclusions. ABil and MC coordinated the experiment. MC

and ABos led the fieldwork. MC, ABos, ACor, CGC, ACon, ACos, GD, GL, LG, LP, and TS participated to the Seismofaults 2017 marine campaign on board the R/V Minerva Uno. Data were mostly processed by MC, ABos, CGC, ACon, ACor, EM, FI, GL, LP, ML, and AP. The manuscript was mostly written by ABil with contributions from all authors. Figures were mostly drawn by MC, ABos, CGC, ACon, EM, LP, and AP with contributions from all authors.

5 *Competing interests.* The authors declare that they have no conflict of interest.

Acknowledgements. With this paper, we release 4970 km^2 of newly-acquired (during the Seismofaults 2017 cruise) high-resolution bathymetric data in numerical form for the Ionian Sea including the BMV (Fig. S1). M. Barbieri, L. Beranzoli, F. Frugoni, S. Monna, and many other colleagues from CNR, INGV, and Sapienza University of Rome are thanked for help and constructive exchanges. The officers and the crew of the R/V Minerva Uno and the scientific party of the Seismofaults 2017 survey are thanked for their cooperation during fieldwork.

10   Some of the figures were produced with the Generic Mapping Tools software (http://gmt.soest.hawaii.edu).

References

Annunziatellis, A., Beaubien, S., Ciotoli, G., Finoia, M., Graziani, S., and Lombardi, S.: Development of an innovative marine monitoring system for CO2 leaks: system design and testing, Energy Procedia, 1, 2333–2340, https://doi.org/10.1016/j.egypro.2009.01.303, 2009.

Argnani, A. and Bonazzi, C.: Malta Escarpment fault zone offshore eastern Sicily: Pliocene-Quaternary tectonic evolution based on new multichannel seismic data, Tectonics, 24, https://doi.org/10.1029/2004TC001656, 2005.

Argnani, A., Brancolini, G., Bonazzi, C., Rovere, M., Accaino, F., Zgur, F., and Lodolo, E.: The results of the Taormina 2006 seismic survey: possible implications for active tectonics in the Messina Straits, Tectonophysics, 476, 159–169, https://doi.org/10.1016/j.tecto.2008.10.029, 2009.

Barber, P. M.: Messinian subaerial erosion of the proto-Nile Delta, Marine Geology, 44, 253–272, https://doi.org/10.1016/0025-3227(81)90053-0, 1981.

Barberio, M. D., Barbieri, M., Billi, A., Doglioni, C., and Petitta, M.: Hydrogeochemical changes before and during the 2016 Amatrice-Norcia seismic sequence (central Italy), Scientific reports, 7, 11 735, https://doi.org/10.1038/s41598-017-11990-8, 2017.

Barnard, A., Sager, W., Snow, J., and Max, M.: Subsea gas emissions from the Barbados Accretionary Complex, Marine and Petroleum Geology, 64, 31–42, https://doi.org/10.1016/j.marpetgeo.2015.02.008, 2015.

Bertoni, C. and Cartwright, J.: Messinian evaporites and fluid flow, Marine and Petroleum Geology, 66, 165–176, https://doi.org/10.1016/j.marpetgeo.2015.02.003, 2015.

Billi, A., Funiciello, R., Minelli, L., Faccenna, C., Neri, G., Orecchio, B., and Presti, D.: On the cause of the 1908 Messina tsunami, southern Italy, Geophysical Research Letters, 35, https://doi.org/10.1029/2008GL033251, 2008.

Billi, A., Minelli, L., Orecchio, B., and Presti, D.: Constraints to the cause of three historical tsunamis (1908, 1783, and 1693) in the Messina Straits region, Sicily, southern Italy, Seismological Research Letters, 81, 907–915, https://doi.org/10.1785/gssrl.81.6.907, 2010.

Billi, A., Faccenna, C., Bellier, O., Minelli, L., Neri, G., Piromallo, C., Presti, D., Scrocca, D., and Serpelloni, E.: Recent tectonic reorganization of the Nubia-Eurasia convergent boundary heading for the closure of the western Mediterranean, Bulletin de la Société Géologique de France, 182, 279–303, https://doi.org/10.2113/gssgfbull.182.4.279, 2011.

Bortoluzzi, G., Faccenna, C., Torelli, L., Artoni, A., Carlini, M., Carone, S., Carrara, G., Cuffaro, M., Ferrante, V., Gasperini, L., et al.: Styles and rates of deformation in the frontal accretionary wedge of the Calabrian Arc (Ionian Sea): controls exerted by the structure of the lower African plate, Italian Journal of Geosciences, 136, 347–364, 2017.

Bosman, A., Casalbore, D., Anzidei, M., Muccini, F., Carmisciano, C., Francesco Latino, C., et al.: The first ultra-high resolution Digital Terrain Model of the shallow-water sector around Lipari Island (Aeolian Islands, Italy), Annals of Geophysics, 58, 2015.

Camerlenghi, A. and Pini, G. A.: Mud volcanoes, olistostromes and Argille scagliose in the Mediterranean region, Sedimentology, 56, 319–365, https://doi.org/10.1111/j.1365-3091.2008.01016.x, 2009.

Camerlenghi, A., Cita, M., Hieke, W., and Ricchiuto, T.: Geological evidence for mud diapirism on the Mediterranean Ridge accretionary complex, Earth and Planetary Science Letters, 109, 493–504, https://doi.org/10.1016/0012-821X(92)90109-9, 1992.

Camerlenghi, A., Cita, M., Della Vedova, B., Fusi, N., Mirabile, L., and Pellis, G.: Geophysical evidence of mud diapirism on the Mediterranean Ridge accretionary complex, Marine Geophysical Researches, 17, 115–141, 1995.

Capozzi, R., Artoni, A., Torelli, L., Lorenzini, S., Oppo, D., Mussoni, P., and Polonia, A.: Neogene to Quaternary tectonics and mud diapirism in the Gulf of Squillace (Crotone-Spartivento Basin, Calabrian Arc, Italy), Marine and Petroleum Geology, 35, 219–234, https://doi.org/10.1016/j.marpetgeo.2012.01.007, 2012.

Capraro, L., Consolaro, C., Fornaciari, E., Massari, F., and Rio, D.: Chronology of the Middle-Upper Pliocene succession in the Strongoli area: constraints on the geological evolution of the Crotone Basin (Southern Italy), Geological Society, London, Special Publications, 262, 323–336, https://doi.org/10.1144/GSL.SP.2006.262.01.19, 2006.

Ceramicola, S., Praeg, D., Cova, A., Accettella, D., and Zecchin, M.: Seafloor distribution and last glacial to postglacial activity of mud volcanoes on the Calabrian accretionary prism, Ionian Sea, Geo-Marine Letters, 34, 111–129, https://doi.org/10.1007/s00367-013-0354-y, 2014.

Cernobori, L., Hirn, A., McBride, J., Nicolich, R., Petronio, L., Romanelli, M., et al.: Crustal image of the Ionian basin and its Calabrian margins, Tectonophysics, 264, 175–189, https://doi.org/10.1016/S0040-1951(96)00125-4, 1996.

Chamot-Rooke, N., Rangin, C., Le Pichon, X., working group, D., et al.: Deep Offshore Tectonics of the Eastern Mediterranean: A Synthesis of Deep Marine Data in the Eastern Mediterranean: the Ionian Basin and Margins, the Calabria Wedge and the Mediterranean Ridge, Société géologique de France, 2005.

Cita, M., Camerlenghi, A., Erba, E., McCoy, F., Castradori, D., Cazzani, A., Guasti, G., Giambastiani, G., Lucchi, R., Nolli, V., et al.: Discovery of mud diapirism on the Mediterranean ridge; a preliminary report, Bollettino della Società Geologica Italiana, 108, 537–543, 1989.

Cita, M., Erba, E., Lucchi, R., Pott, M., Van der Meer, R., and Nieto, L.: Stratigraphy and sedimentation in the Mediterranean Ridge diapiric belt, Marine Geology, 132, 131–150, https://doi.org/10.1016/0025-3227(96)00157-0, 1996.

Cita, M. B.: Prometheus mud breccia: an example of shale diapirism in the western Mediterranean ridge, in: Annales geologiques des Pays helleniques, vol. 30, pp. 543–569, 1981.

Claesson, L., Skelton, A., Graham, C., Dietl, C., Morth, M., Torssander, P., and Kockum, I.: Hydrogeochemical changes before and after a major earthquake, Geology, 32, 641–644, https://doi.org/10.1130/G20542.1, 2004.

Deville, E., Battani, A., Griboulard, R., Guerlais, S., Herbin, J., Houzay, J., Muller, C., and Prinzhofer, A.: The origin and processes of mud volcanism: new insights from Trinidad, Geological Society, London, Special Publications, 216, 475–490, https://doi.org/10.1144/GSL.SP.2003.216.01.31, 2003.

Dimitrov, L. I.: Mud volcanoes—the most important pathway for degassing deeply buried sediments, Earth-Science Reviews, 59, 49–76, https://doi.org/10.1016/S0012-8252(02)00069-7, 2002.

Doglioni, C., Ligi, M., Scrocca, D., Bigi, S., Bortoluzzi, G., Carminati, E., Cuffaro, M., D'oriano, F., Forleo, V., Muccini, F., et al.: The tectonic puzzle of the Messina area (Southern Italy): Insights from new seismic reflection data, Scientific reports, 2, 970, https://doi.org/10.1038/srep00970, 2012.

Etiope, G. and Milkov, A. V.: A new estimate of global methane flux from onshore and shallow submarine mud volcanoes to the atmosphere, Environmental Geology, 46, 997–1002, https://doi.org/10.1007/s00254-004-1085-1, 2004.

Evans, R. J., Stewart, S. A., and Davies, R. J.: The structure and formation of mud volcano summit calderas, Journal of the Geological Society, 165, 769–780, https://doi.org/10.1144/0016-76492007-118, 2008.

Faccenna, C., Becker, T. W., Auer, L., Billi, A., Boschi, L., Brun, J. P., Capitanio, F. A., Funiciello, F., Horvàth, F., Jolivet, L., et al.: Mantle dynamics in the Mediterranean, Reviews of Geophysics, 52, 283–332, https://doi.org/10.1002/2013RG000444, 2014.

Gallais, F., Gutscher, M.-A., Klaeschen, D., and Graindorge, D.: Two-stage growth of the Calabrian accretionary wedge in the Ionian Sea (Central Mediterranean): Constraints from depth-migrated multichannel seismic data, Marine Geology, 326, 28–45, https://doi.org/10.1016/j.margeo.2012.08.006, 2012.

Gallais, F., Graindorge, D., Gutscher, M.-A., and Klaeschen, D.: Propagation of a lithospheric tear fault (STEP) through the western boundary of the Calabrian accretionary wedge offshore eastern Sicily (Southern Italy), Tectonophysics, 602, 141–152, https://doi.org/10.1016/j.tecto.2012.12.026, 2013.

Gamberi, F. and Rovere, M.: Mud diapirs, mud volcanoes and fluid flow in the rear of the Calabrian Arc Orogenic Wedge (southeastern Tyrrhenian sea), Basin Research, 22, 452–464, https://doi.org/10.1111/j.1365-2117.2010.00473.x, 2010.

Gennari, G., Spezzaferri, S., Comas, M., Rüggeberg, A., Lopez-Rodriguez, C., and Pinheiro, L.: Sedimentary sources of the mud-breccia and mud volcanic activity in the Western Alboran Basin, Marine Geology, 339, 83–95, https://doi.org/10.1016/j.margeo.2013.04.002, 2013.

Gutscher, M.-A., Dominguez, S., de Lepinay, B. M., Pinheiro, L., Gallais, F., Babonneau, N., Cattaneo, A., Le Faou, Y., Barreca, G., Micallef, A., et al.: Tectonic expression of an active slab tear from high-resolution seismic and bathymetric data offshore Sicily (Ionian Sea), Tectonics, 35, 39–54, https://doi.org/10.1002/2015TC003898, 2016.

Gutscher, M.-A., Kopp, H., Krastel, S., Bohrmann, G., Garlan, T., Zaragosi, S., Klaucke, I., Wintersteller, P., Loubrieu, B., Le Faou, Y., et al.: Active tectonics of the Calabrian subduction revealed by new multi-beam bathymetric data and high-resolution seismic profiles in the Ionian Sea (Central Mediterranean), Earth and Planetary Science Letters, 461, 61–72, https://doi.org/10.1016/j.epsl.2016.12.020, 2017.

Higgins, G.: Mud volcanoes, their nature and origin, Verh. Naturfsch. Ges. Basel, 84, 101–152, 1974.

Hilton, D. R.: The helium and carbon isotope systematics of a continental geothermal system: results from monitoring studies at Long Valley caldera (California, USA), Chemical Geology, 127, 269–295, https://doi.org/10.1016/0009-2541(95)00134-4, 1996.

Huang, F., Li, M., Ma, Y., Han, Y., Tian, L., Yan, W., and Li, X.: Studies on earthquake precursors in China: A review for recent 50 years, Geodesy and Geodynamics, 8, 1–12, https://doi.org/10.1016/j.geog.2016.12.002, 2017.

Huang, Q. and Ding, X.: Spatiotemporal variations of seismic quiescence prior to the 2011 M 9.0 Tohoku earthquake revealed by an improved Region–Time–Length algorithm, Bulletin of the Seismological Society of America, 102, 1878–1883, https://doi.org/10.1785/0120110343, 2012.

Igarashi, G., Saeki, S., Takahata, N., Sumikawa, K., Tasaka, S., Sasaki, Y., Takahashi, M., and Sano, Y.: Ground-water radon anomaly before the Kobe earthquake in Japan, Science, 269, 60–61, https://doi.org/10.1126/science.269.5220.60, 1995.

Inan, S., Balderer, W. P., Leuenberger-West, F., Yakan, H., Özvan, A., and Freund, F. T.: Springwater chemical anomalies prior to the Mw= 7.2 Van earthquake (Turkey), Geochemical Journal, 46, e11–e16, https://doi.org/10.2343/geochemj.1.0159, 2012.

Italiano, F., Martinelli, G., and Nuccio, P.: Anomalies of mantle-derived helium during the 1997–1998 seismic swarm of Umbria-Marche, Italy, Geophysical Research Letters, 28, 839–842, https://doi.org/10.1029/2000GL012059, 2001.

Italiano, F., Bonfanti, P., Ditta, M., Petrini, R., and Slejko, F.: Helium and carbon isotopes in the dissolved gases of Friuli region (NE Italy): geochemical evidence of CO_2 production and degassing over a seismically active area, Chemical Geology, 266, 76–85, https://doi.org/10.1016/j.chemgeo.2009.05.022, 2009.

Italiano, F., Yuce, G., Uysal, I., Gasparon, M., and Morelli, G.: Insights into mantle-type volatiles contribution from dissolved gases in artesian waters of the Great Artesian Basin, Australia, Chemical geology, 378, 75–88, https://doi.org/10.1016/j.chemgeo.2014.04.013, 2014.

King, C.-Y., Koizumi, N., and Kitagawa, Y.: Hydrogeochemical anomalies and the 1995 Kobe earthquake, Science, 269, 38–40, 1995.

Kioka, A. and Ashi, J.: Episodic massive mud eruptions from submarine mud volcanoes examined through topographical signatures, Geophysical Research Letters, 42, 8406–8414, https://doi.org/10.1016/j.margeo.2015.01.014, 2015.

Kioka, A., Ashi, J., Sakaguchi, A., Sato, T., Muraoka, S., Yamaguchi, A., Hamamoto, H., Wang, K., and Tokuyama, H.: Possible mechanism of mud volcanism at the prism-backstop contact in the western Mediterranean Ridge Accretionary Complex, Marine Geology, 363, 52–64, https://doi.org/10.1016/j.margeo.2015.01.014, 2015.

Kirkham, C., Cartwright, J., Hermanrud, C., and Jebsen, C.: The spatial, temporal and volumetric analysis of a large mud volcano province within the Eastern Mediterranean, Marine and Petroleum Geology, 81, 1–16, https://doi.org/10.1016/j.marpetgeo.2016.12.026, 2017.

Kopf, A., Robertson, A., Clennell, M., and Flecker, R.: Mechanisms of mud extrusion on the Mediterranean Ridge Accretionary Complex, Geo-Marine Letters, 18, 97–114, 1998.

Kopf, A. J.: Significance of mud volcanism, Reviews of Geophysics, 40, 2–1, https://doi.org/10.1029/2000RG000093, 2002.

León, R., Somoza, L., Medialdea, T., González, F., Díaz-del Río, V., Fernández-Puga, M., Maestro, A., and Mata, M.: Sea-floor features related to hydrocarbon seeps in deepwater carbonate-mud mounds of the Gulf of Cádiz: from mud flows to carbonate precipitates, Geo-Marine Letters, 27, 237–247, https://doi.org/10.1007/s00367-007-0074-2, 2007.

Limonov, A., Woodside, J., Cita, M., and Ivanov, M.: The Mediterranean Ridge and related mud diapirism: a background, Marine Geology, 132, 7–19, https://doi.org/10.1016/0025-3227(96)00150-8, 1996.

Locati, M., CCamassi, R. D., Rovida, A. N., Ercolani, E., Bernardini, F. M. A., Castelli, V., Caracciolo, C. H., Tertulliani, A., Rossi, A., Azzaro, R., et al.: DBMI15, the 2015 version of the Italian Macroseismic Database. Istituto Nazionale di Geofisica e Vulcanologia, 2016.

Loher, M., Ceramicola, S., Wintersteller, P., Meinecke, G., Sahling, H., and Bohrmann, G.: Mud volcanism in a canyon: Morphodynamic evolution of the active Venere mud volcano and its interplay with Squillace Canyon, Central Mediterranean, Geochemistry, Geophysics, Geosystems, 19, 356–378, https://doi.org/10.1002/2017GC007166, 2018.

Martinelli, G. and Ferrari, G.: Earthquake forerunners in a selected area of Northern Italy: recent developments in automatic geochemical monitoring, Tectonophysics, 193, 397–410, https://doi.org/10.1016/0040-1951(91)90348-V, 1991.

Martinelli, G., Albarello, D., and Mucciarelli, M.: Radon emissions from mud volcanoes in Northern Italy: possible connection with local seismicity, Geophysical research letters, 22, 1989–1992, https://doi.org/10.1029/95GL01785, 1995.

Mazzini, A. and Etiope, G.: Mud volcanism: an updated review, Earth-science reviews, 168, 81–112, https://doi.org/10.1016/j.earscirev.2017.03.001, 2017.

Mazzini, A., Svensen, H., Akhmanov, G., Aloisi, G., Planke, S., Malthe-Sørenssen, A., and Istadi, B.: Triggering and dynamic evolution of the LUSI mud volcano, Indonesia, Earth and Planetary Science Letters, 261, 375–388, https://doi.org/10.1016/j.epsl.2007.07.001, 2007.

Mazzini, A., Svensen, H., Planke, S., Guliyev, I., Akhmanov, G., Fallik, T., and Banks, D.: When mud volcanoes sleep: insight from seep geochemistry at the Dashgil mud volcano, Azerbaijan, Marine and Petroleum Geology, 26, 1704–1715, https://doi.org/10.1016/j.marpetgeo.2008.11.003, 2009.

Milkov, A.: Worldwide distribution of submarine mud volcanoes and associated gas hydrates, Marine Geology, 167, 29–42, https://doi.org/10.1016/S0025-3227(00)00022-0, 2000.

Milkov, A. V., Sassen, R., Apanasovich, T. V., and Dadashev, F. G.: Global gas flux from mud volcanoes: a significant source of fossil methane in the atmosphere and the ocean, Geophysical Research Letters, 30, https://doi.org/10.1029/2002GL016358, 2003.

Minelli, L. and Faccenna, C.: Evolution of the Calabrian accretionary wedge (central Mediterranean), Tectonics, 29, https://doi.org/10.1029/2009TC002562, 2010.

Onda, S., Sano, Y., Takahata, N., Kagoshima, T., Miyajima, T., Shibata, T., Pinti, D. L., Lan, T., Kim, N. K., Kusakabe, M., et al.: Groundwater oxygen isotope anomaly before the M6. 6 Tottori earthquake in Southwest Japan, Scientific reports, 8, 4800, https://doi.org/10.1038/s41598-018-23303-8, 2018.

Orecchio, B., Presti, D., Totaro, C., and Neri, G.: What earthquakes say concerning residual subduction and STEP dynamics in the Calabrian Arc region, south Italy, Geophysical Journal International, 199, 1929–1942, https://doi.org/10.1093/gji/ggu373, 2014.

Palano, M., Ferranti, L., Monaco, C., Mattia, M., Aloisi, M., Bruno, V., Cannavò, F., and Siligato, G.: GPS velocity and strain fields in Sicily and southern Calabria, Italy: updated geodetic constraints on tectonic block interaction in the central Mediterranean, Journal of Geophysical Research: Solid Earth, 117, https://doi.org/10.1029/2012JB009254, 2012.

Palano, M., Schiavone, D., Loddo, M., Neri, M., Presti, D., Quarto, R., Totaro, C., and Neri, G.: Active upper crust deformation pattern along the southern edge of the Tyrrhenian subduction zone (NE Sicily): Insights from a multidisciplinary approach, Tectonophysics, 657, 205–218, https://doi.org/10.1016/j.tecto.2015.07.005, 2015.

Panieri, G., Polonia, A., Lucchi, R., Zironi, S., Capotondi, L., Negri, A., and Torelli, L.: Mud volcanoes along the inner deformation front of the Calabrian Arc accretionary wedge (Ionian Sea), Marine Geology, 336, 84–98, https://doi.org/10.1016/j.margeo.2012.11.003, 2013.

Patacca, E. and Scandone, P.: The 1627 Gargano earthquake (Southern Italy): identification and characterization of the causative fault, Journal of Seismology, 8, 259–273, https://doi.org/10.1023/B:JOSE.0000021393.77543.1e, 2004.

Petitta, M., Mastrorillo, L., Preziosi, E., Banzato, F., Barberio, M. D., Billi, A., Cambi, C., De Luca, G., Di Carlo, G., Di Curzio, D., et al.: Water-table and discharge changes associated with the 2016-2017 seismic sequence in central Italy: hydrogeological data and a conceptual model for fractured carbonate aquifers, Hydrogeology Journal, pp. 1–18, https://doi.org/10.1007/s10040-017-1717-7, 2018.

Planke, S., Svensen, H., Hovland, M., Banks, D., and Jamtveit, B.: Mud and fluid migration in active mud volcanoes in Azerbaijan, Geo-Marine Letters, 23, 258–268, https://doi.org/10.1007/s00367-003-0152-z, 2003.

Polonia, A., Torelli, L., Mussoni, P., Gasperini, L., Artoni, A., and Klaeschen, D.: The Calabrian Arc subduction complex in the Ionian Sea: Regional architecture, active deformation, and seismic hazard, Tectonics, 30, https://doi.org/10.1029/2010TC002821, 2011.

Polonia, A., Torelli, L., Gasperini, L., and Mussoni, P.: Active faults and historical earthquakes in the Messina Straits area (Ionian Sea), Natural Hazards and Earth system sciences, 12, 2311–2328, https://doi.org/10.5194/nhess-12-2311-2012, 2012.

Polonia, A., Torelli, L., Artoni, A., Carlini, M., Faccenna, C., Ferranti, L., Gasperini, L., Govers, R., Klaeschen, D., Monaco, C., et al.: The Ionian and Alfeo–Etna fault zones: New segments of an evolving plate boundary in the central Mediterranean Sea?, Tectonophysics, 675, 69–90, https://doi.org/10.1016/j.tecto.2016.03.016, 2016.

Polonia, A., Nelson, C., Romano, S., Vaiani, S., Colizza, E., Gasparotto, G., and Gasperini, L.: A depositional model for seismo-turbidites in confined basins based on Ionian Sea deposits, Marine Geology, 384, 177–198, https://doi.org/10.1016/j.margeo.2016.05.010, 2017.

Praeg, D., Ceramicola, S., Barbieri, R., Unnithan, V., and Wardell, N.: Tectonically-driven mud volcanism since the late Pliocene on the Calabrian accretionary prism, central Mediterranean Sea, Marine and Petroleum Geology, 26, 1849–1865, https://doi.org/10.1016/j.marpetgeo.2009.03.008, 2009.

Rabaute, A. and Chamot-Rooke, N.: Quantitative mapping of active mud volcanism at the western Mediterranean Ridge-backstop contact, Marine Geophysical Researches, 28, 271–295, https://doi.org/10.1007/s11001-007-9031-8, 2007.

Roberts, J. J., Gilfillan, S. M., Stalker, L., and Naylor, M.: Geochemical tracers for monitoring offshore CO 2 stores, International Journal of Greenhouse Gas Control, 65, 218–234, https://doi.org/10.1016/j.ijggc.2017.07.021, 2017.

Robertson, A.: Mud volcanism on the Mediterranean Ridge: Initial results of ocean drilling program Leg 160, Geology, 24, 239–242, https://doi.org/10.1130/0091-7613(1996)024<0239:MVOTMR>2.3.CO;2, 1996.

Robertson, A. H. and Kopf, A.: Tectonic setting and processes of mud volcanism on the Mediterranean Ridge accretionary complex: evidence from Leg 160., Proceedings of the Ocean Drilling Program, Scientific Results, Vol. 160; Chapter 50, 1998.

Römer, M., Sahling, H., Pape, T., dos Santos Ferreira, C., Wenzhöfer, F., Boetius, A., and Bohrmann, G.: Methane fluxes and carbonate deposits at a cold seep area of the Central Nile Deep Sea Fan, Eastern Mediterranean Sea, Marine Geology, 347, 27–42, https://doi.org/10.1016/j.margeo.2013.10.011, 2014.

Rossi, S. and Sartori, R.: A seismic reflection study of the external Calabrian Arc in the northern Ionian Sea (eastern Mediterranean), Marine Geophysical Researches, 4, 403–426, 1981.

Rovere, M., Gamberi, F., Mercorella, A., Rashed, H., Gallerani, A., Leidi, E., Marani, M., Funari, V., and Pini, G. A.: Venting and seepage systems associated with mud volcanoes and mud diapirs in the southern Tyrrhenian Sea, Marine Geology, 347, 153–171, https://doi.org/10.1016/j.margeo.2013.11.013, 2014.

Sano, Y. and Wakita, H.: Precise measurement of helium isotopes in terrestrial gases, Bulletin of the Chemical Society of Japan, 61, 1153–1157, 1988.

Sano, Y., Takahata, N., Kagoshima, T., Shibata, T., Onoue, T., and Zhao, D.: Groundwater helium anomaly reflects strain change during the 2016 Kumamoto earthquake in Southwest Japan, Scientific Reports, 6, 37 939, https://doi.org/10.1038/srep37939, 2016.

Scrocca, D., Doglioni, C., and Innocenti, F.: Constraints for an interpretation of the Italian geodynamics: a review, Memorie Descrittive della Carta Geologica d Italia, 62, 15–46, 2003.

Sella, P., Billi, A., Mazzini, I., De Filippis, L., Pizzino, L., Sciarra, A., and Quattrocchi, F.: A newly-emerged (August 2013) artificially-triggered fumarole near the Fiumicino airport, Rome, Italy, Journal of Volcanology and Geothermal Research, 280, 53–66, https://doi.org/10.1016/j.jvolgeores.2014.05.008, 2014.

Serpelloni, E., Vannucci, G., Pondrelli, S., Argnani, A., Casula, G., Anzidei, M., Baldi, P., and Gasperini, P.: Kinematics of the Western Africa-Eurasia plate boundary from focal mechanisms and GPS data, Geophysical Journal International, 169, 1180–1200, https://doi.org/10.1111/j.1365-246X.2007.03367.x, 2007.

Skelton, A., Claesson, L., Chakrapani, G., Mahanta, C., Routh, J., Mörth, M., and Khanna, P.: Coupling between seismic activity and hydrogeochemistry at the Shillong Plateau, Northeastern India, Pure and Applied Geophysics, 165, 45–61, https://doi.org/10.1007/s00024-007-0288-2, 2008.

Skelton, A., Andrén, M., Kristmannsdóttir, H., Stockmann, G., Mörth, C.-M., Sveinbjörnsdóttir, Á., Jónsson, S., Sturkell, E., Guðrúnardóttir, H. R., Hjartarson, H., et al.: Changes in groundwater chemistry before two consecutive earthquakes in Iceland, Nature Geoscience, 7, 752, https://doi.org/10.1038/NGEO2250, 2014.

Somoza, L., Medialdea, T., León, R., Ercilla, G., Vázquez, J. T., Hernández-Molina, J., González, J., Juan, C., Fernández-Puga, M. C., et al.: Structure of mud volcano systems and pockmarks in the region of the Ceuta Contourite Depositional System (Western Alborán Sea), Marine Geology, 332, 4–26, https://doi.org/10.1016/j.margeo.2012.06.002, 2012.

Staffini, F., Spezzaferri, S., and Aghib, F.: Mud diapirs of the Mediterranean Ridge: sedimentological and micropaleontological study of the mud breccia, Rivista Italiana di Paleontologia e Stratigrafia (Research In Paleontology and Stratigraphy), 99, 1993.

Totaro, C., Presti, D., Billi, A., Gervasi, A., Orecchio, B., Guerra, I., and Neri, G.: The ongoing seismic sequence at the Pollino Mountains, Italy, Seismological Research Letters, 84, 955–962, https://doi.org/10.1785/0220120194, 2013.

Tung, S. and Masterlark, T.: Delayed poroelastic triggering of the 2016 October Visso earthquake by the August Amatrice earthquake, Italy, Geophysical Research Letters, 45, 2221–2229, https://doi.org/10.1002/2017GL076453, 2018.

Valensise, G. and Pantosti, D.: A 125 Kyr-long geological record of seismic source repeatability: the Messina Straits (southern Italy) and the 1908 earthquake (Ms 7 1/2), Terra Nova, 4, 472–483, https://doi.org/10.1111/j.1365-3121.1992.tb00583.x, 1992.

van der Meer, R.: Grading in mud volcanic breccia from the Mediterranean Ridge, Marine geology, 132, 165–173, https://doi.org/10.1016/0025-3227(95)00159-X, 1996.

Wakita, H., Nakamura, Y., and Sano, Y.: Short-term and intermediate-term geochemical precursors, Pure and applied geophysics, 126, 267–278, 1988.

5 Wortel, M. and Spakman, W.: Subduction and slab detachment in the Mediterranean-Carpathian region, Science, 290, 1910–1917, https://doi.org/10.1126/science.290.5498.1910, 2000.
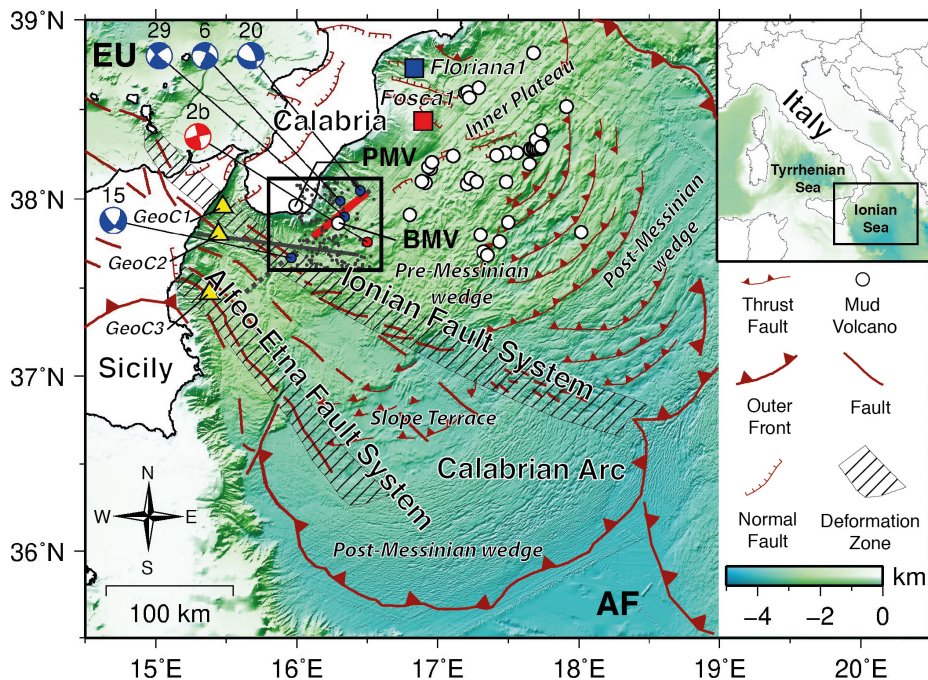
Figure 1. Bathymetric map the Ionian Sea (southern Italy) with main faults, mud volcanoes, earthquakes, tracks of multichannel seismic profiles, and location of the Fosca 1 (red square) and Floriana 1 (blue square) offshore wells. Location of mud volcanoes (except PMV) are from Loher et al. (2018). The Bortoluzzi Mud Volcano is indicated with BMV. The Palizzi mud volcano (onland Calabria) is indicated with PMV. Grey thick line corresponds to the CROP M-31 multichannel seismic profile (Fig. 10a). Grey dashed line and thick red line are the CA99-215 multichannel profile (Fig. 10b) and its close up view reported in Fig. 10(c), respectively. Earthquake data (epicenters are indicated with thin grey dots whereas focal mechanisms with beach balls) surrounding the BMV area are from the European-Mediterranean Regional Centroid-Moment Tensors (RCMT) catalog (http://rcmt2.bo.ingv.it/) (red beach ball) and from previous papers (blue beach balls) by Orecchio et al. (2014) and Polonia et al. (2016). Faults are principally from Polonia et al. (2011), Polonia et al. (2016) and Bortoluzzi et al. (2017). The black box is the location of Fig. 2. AF stands for Africa Plate whereas EU for Eurasia Plate. GeoC1, GeoC2, and GeoC3 are locations of sea water column sampling.
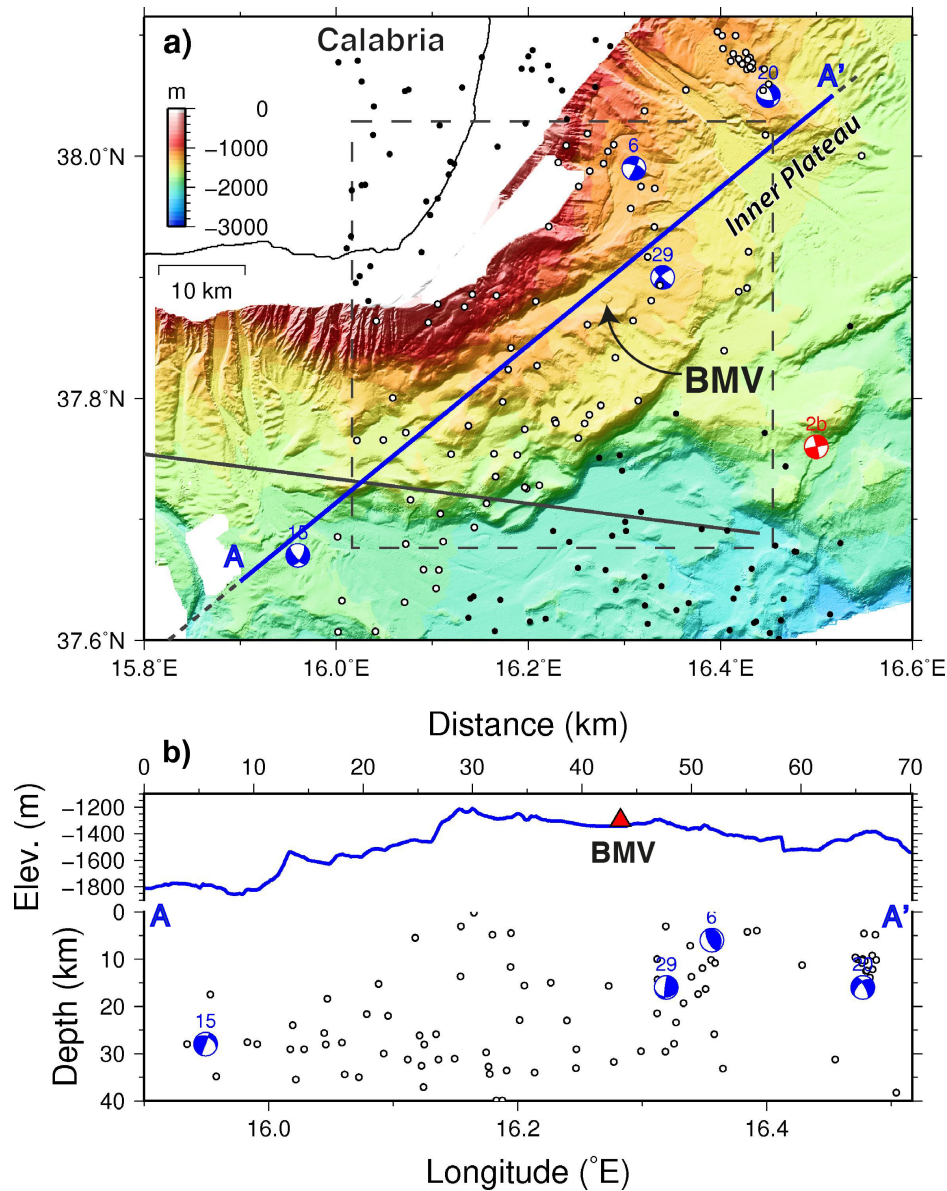
Figure 2. (a) High resolution bathymetry (see location in Fig. 1) of the Calabrian off-shore, Ionian Sea, with location of the BMV. Earthquake epicenters and focal mechanisms (Tables S1 and S2) surrounding the BMV area are shown as dots (black and white) and beach balls, respectively. Focal mechanisms (Table S2) are from the European-Mediterranean Regional Centroid-Moment Tensors (red beach ball) catalog (http://rcmt2.bo.ingv.it/) and from previous papers (blue beach balls) by Orecchio et al. (2014) and Polonia et al. (2016). White dots represent the selected seismic events at distance of 12 km to be projected along the transect A-A' (blue line). Grey thick and grey dashed lines corresponds to the CROP M-31 (Fig. 10b) and the CA99-215 (Fig. 10a) multichannel profiles, respectively. The black dashed box is the location of Fig. 3. (b) A-A' vertical cross-sectional transect (see track in Fig. 2a) showing a perpendicular projection (onto the transect) of earthquake hypocenters and focal mechanisms for the BMV area. The blue line is the corresponding seafloor profile, over which the projected location of the BMV (red triangle) is shown.
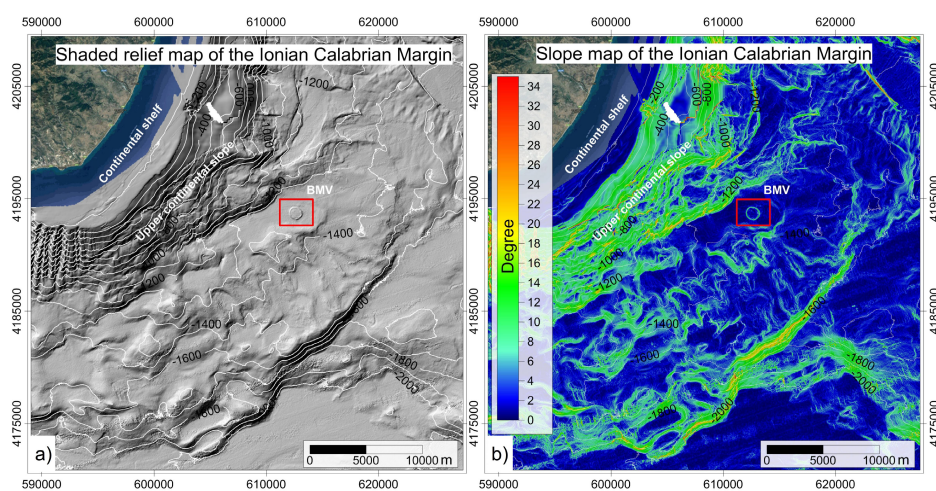
Figure 3. (a) Bathy-morphological map and (b) slope map of the upper portion of the continental slope of the Calabrian-Ionian margin. Red square indicates the intraslope flat area hosting the circular high of the Bortoluzzi Mud Volcano (BMV).
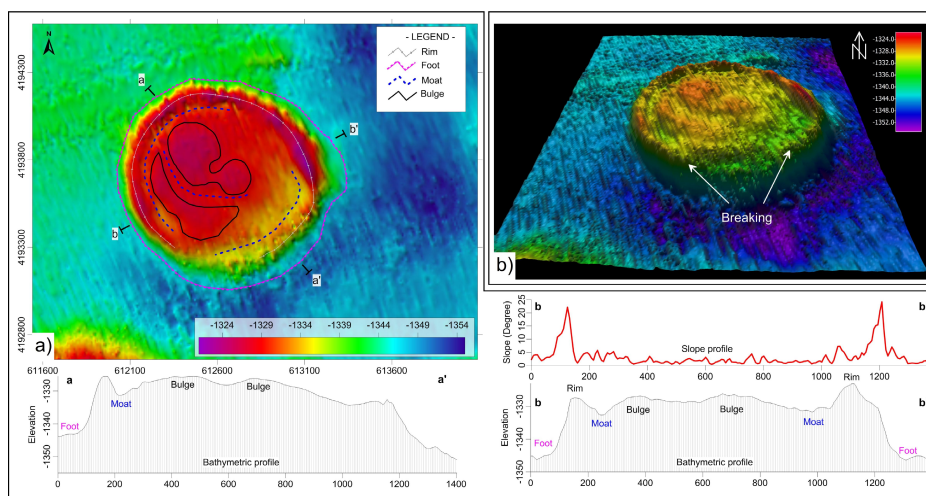
Figure 4. (a) Shaded relief map of the BMV with the main morphological features and location of bathymetric sections (a-a' and b-b'). The map is accompanied by two bathymetric profiles (bottom left and bottom right) along the a-a' and b-b' tracks and by one slope profile (middle right) along the b-b' track. (b) 3D perspective view of the BMV showing some main morphological features.
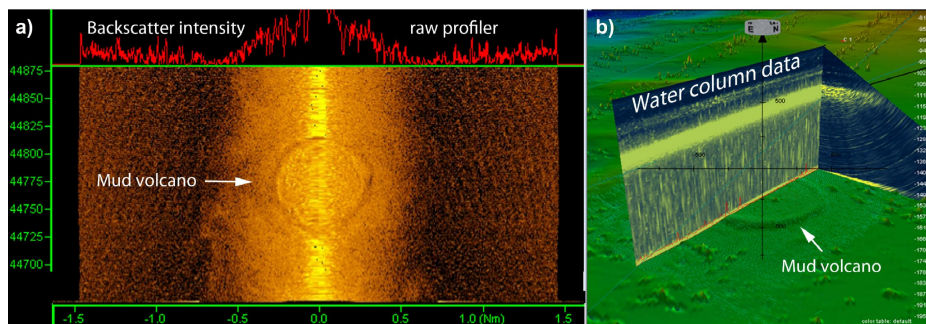
Figure 5. (a) Raw profiler backscatter of the BMV area. (b) Acoustic backscatter of the water column above the BMV. These data show the substantial absence of amplitude anomalies and therefore massive fluid escapes from the seafloor.
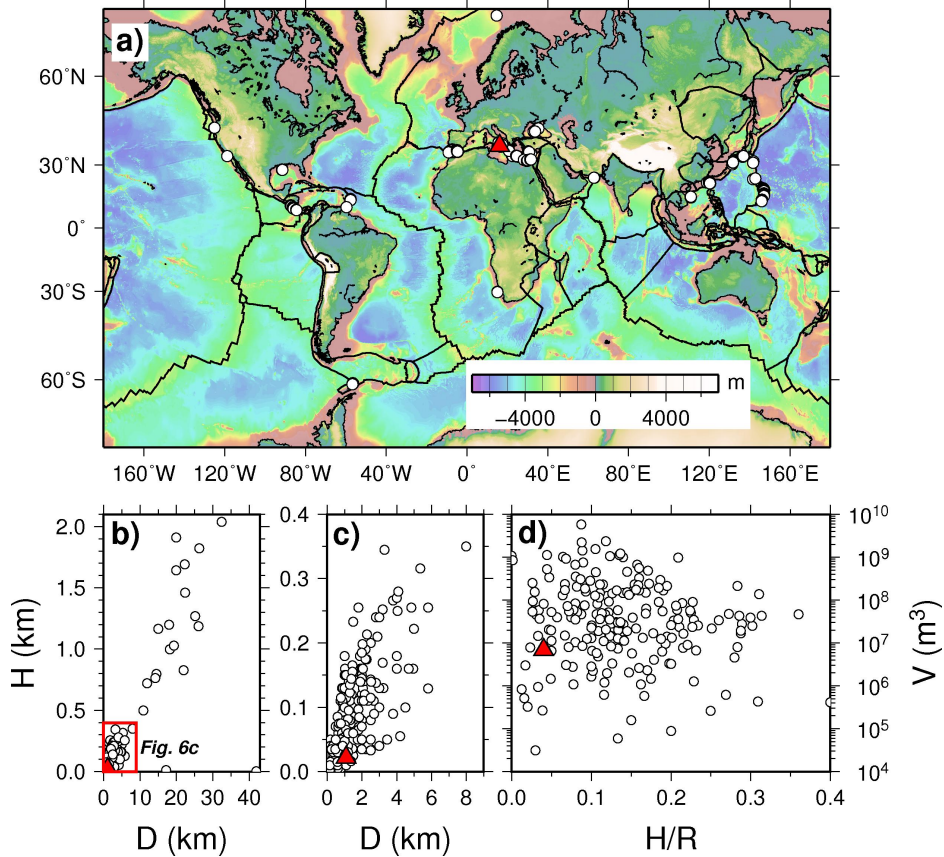
Figure 6. (a) Selection of worldwide distribution of mud volcanoes (white dots) from the dataset reported by Kioka and Ashi (2015). In particular, 232 volcanoes with available mean diameter D and height H are shown. The red triangle is the BMV location. (b) Compilation of mud volcanoes diameter D vs. height H, showing an approximately linear trend between increasing mud volcano diameters and heights, excluding some exceptions. Along this trend, the BMV (red triangle) stands close the lower values. (c) Close-up view of a portion of the diagram in b. (d) Compilation of volumes V of mud volcanoes vs. H/R (where R is the radius of the volcano base), showing that the H/R ratio is ≤ 0.4 for all mud volcanoes, whereas there is a scatter distribution of mud volcano volumes, mostly ranging in the 106-109 m^3 interval. The BMV volume (red triangle) corresponds to 6.9 x106 m^3.
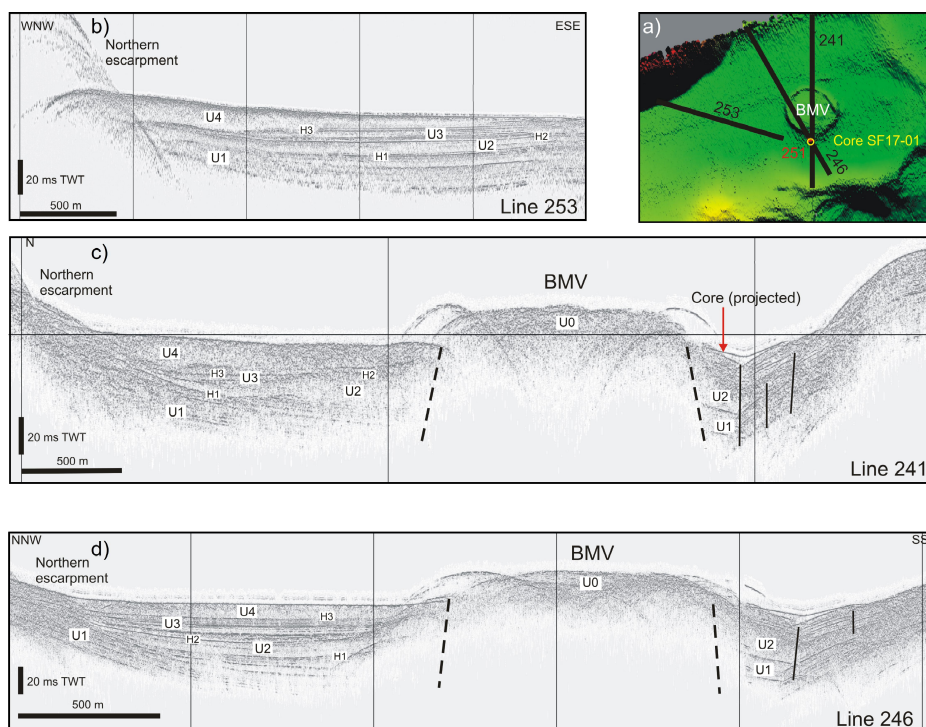
Figure 7. (a) Location map of three single-channel chirp profiles and one gravity core in the BMV area. The red dot (numbered 251) below the location of the gravity core indicates the location of the single-channel chirp profile 251 shown in Fig. 9. (b) Line 253. (c) Line 241. (d) Line 246. Chirp profiles show main seismic units (U0-U4) and bounding horizons identified in the shallow subsurface. The high-resolution non-interpreted version of this figure is available in the Supplement (Fig. S1).
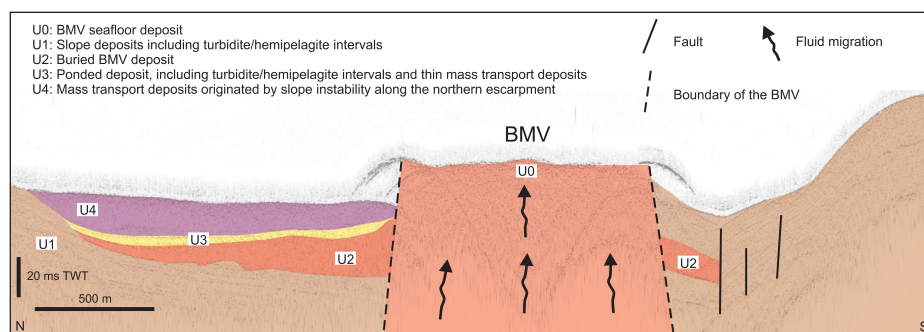
Figure 8. Interpretation of the chirp profile 241 shown in Fig. 7 (see text for details).
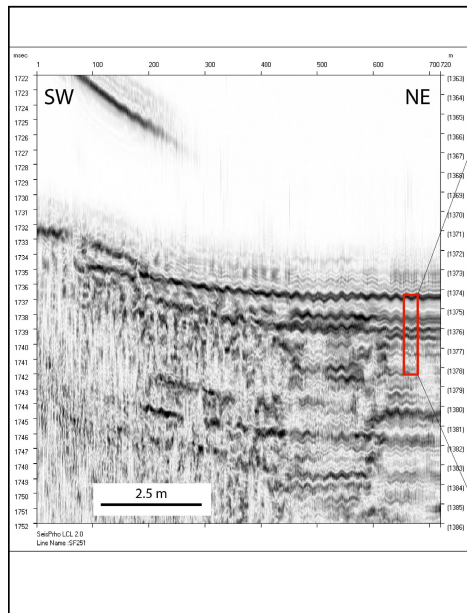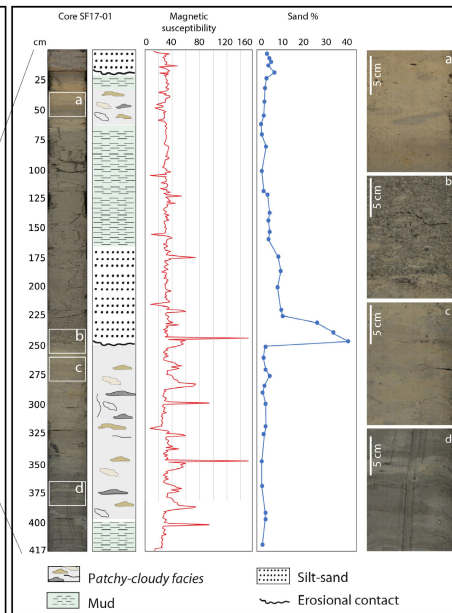
Figure 9. Correlation between the SF17-01 gravity core (right) and the 251 chirp profile (right). See locations in Fig. 7. Left: 251 chirp profile collected during coring operations. Right: photograph, lithological log, high-resolution magnetic susceptibility, and sand content of the SF17-01 gravity core. Magnetic susceptibility is rather constant throughout the core with the exception of some peaks in the lower part of the core, where the patchy-cloudy facies is present. A peak in magnetic susceptibility marks the abrupt increase in sand content at the base of the resedimented deposit between 75 and 250 cm. a, b, c, d represent close-ups of different core units: a, c, and d are patchy cloudy facies whereas b is the base of the resedimented unit.
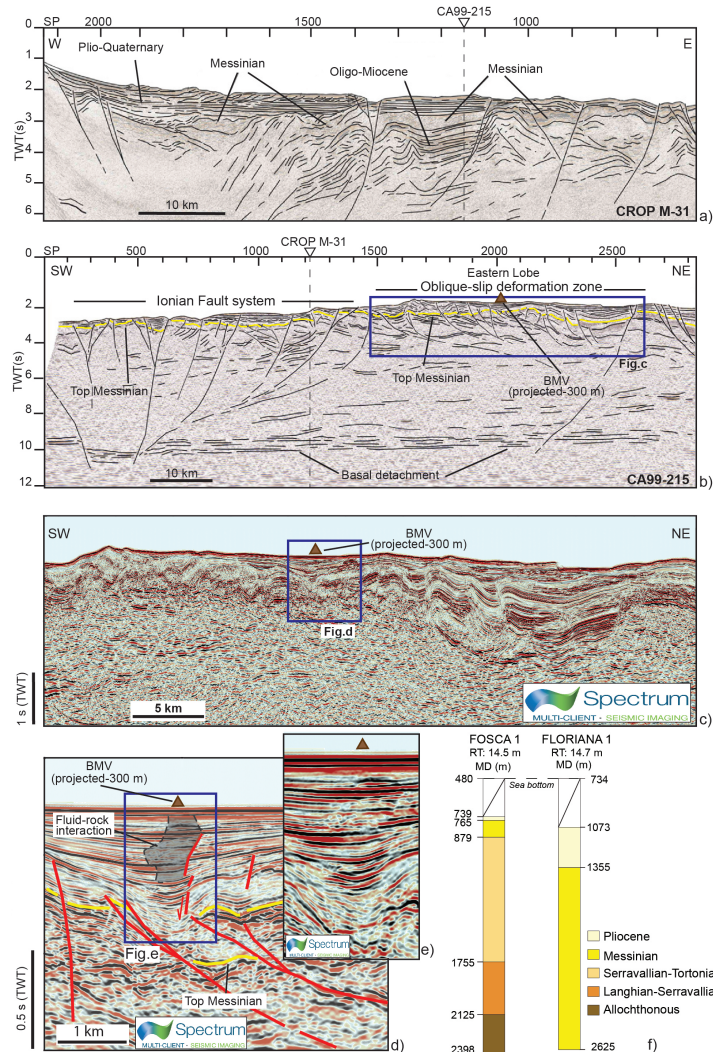
Figure 10. (a) CROP M-31 seismic reflection profiles (track in Fig. 1) in the version interpreted by Polonia et al. (2016), showing the complex structural setting and the main interpreted deposits. The CROP M-31 profile crosses the CA99-215 profile at s.p. 1150. (b) CA99-215 seismic reflection profiles (track in Fig. 1) in the version interpreted by Polonia et al. (2016). The top of the Messinian deposits is reported in yellow. The CA99-215 profile crosses the CROP M-31 profile at s.p. 1210. (c) Portion of the CA99-215 profile reprocessed by Spectrum Geo Ltd (http://www.spectrumgeo.com/). The BMV is projected from a distance of ≃200 m. (d) and (e) Close up views of a portion of the reprocessed CA99-215 profile where the BMV is located. See Fig. S3 for a non-interpreted high-resolution version of Fig. 10(e). Note that the Messinian and Pliocene deposits are faulted by normal and thrust faults. The area just below the projection of the BMV is characterized by a chaotic and slightly transparent seismic reflection signal as is typical beneath many mud volcanoes for the fluid-rock interaction. (f) Stratigraphic syntheses of the Fosca 1 and Floriana 1 wells (see location in Fig. 1). RT: Rotary Table. MD: Measure Depth. Raw well data are from the Videpi free database (available only at http://unmig.sviluppoeconomico.gov.it/videpi/videpi.asp).
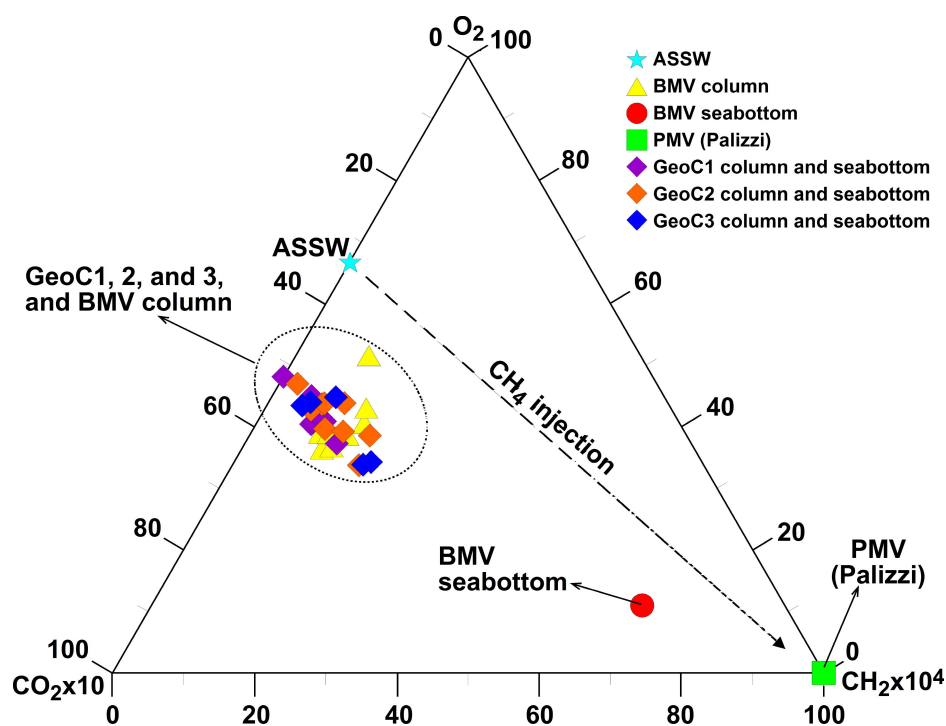
Figure 11. CH_4-O_2-CO_2 diagram. The ternary plot shows relative distribution of dissolved gases for the collected samples. Dissolved gases composition coming from the sampling site above the BMV are compared with the local air-saturated sea water (ASSW). The figure shows typical endogenic components (CO_2 and CH_4) versus the atmospheric component (here represented by O_2).
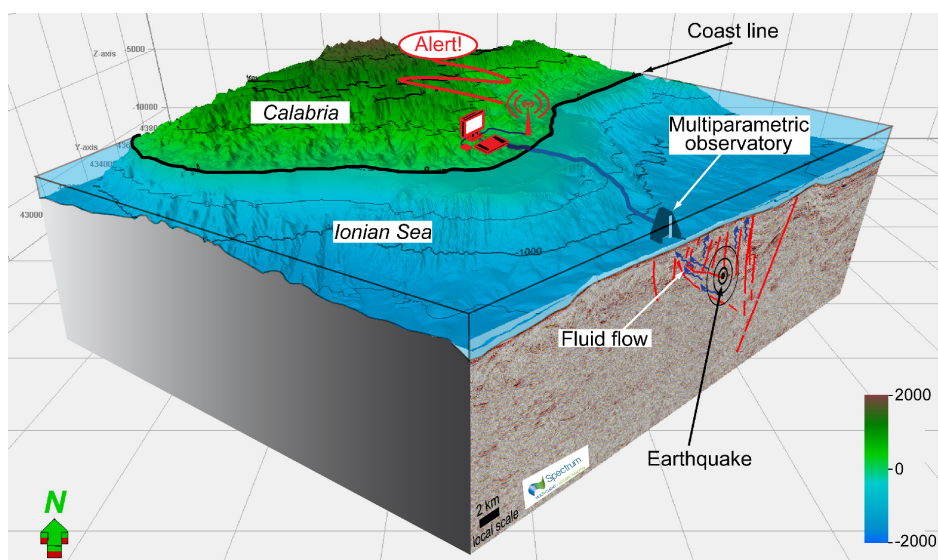
Figure 12. Conceptual scheme showing a future multiparametric cabled station on the BMV to geochemically tracking the seismic cycle of the underlying active faults and so to contribute to the mitigation of the seismic hazard.

Sample	date	depth(m)	Latitude	Longitude	T°C	pH	Na(meq/L)	K(meq/L)	Mg(meq/L)	Ca(meq/L)	Cl(meq/L)	Br(meq/L)	SO_4(meq/L)	HCO_3(meq/L)
GeoC1	05.17.2017	-1043	37°57'24.6"	15°28'29.4"	13.80	8.16	553	12.7	125	24.9	644	0.930	67.1	2.68
GeoC2	05.16.2017	-1649	37°43'10.8"	15°26'40.8"	13.79	8.37	552	12.7	125	25.2	637	0.999	66.5	2.68
GeoC3	05.16.2017	-2029	37°28'10.8"	15°23'01.8"	13.82	8.10	554	12.8	126	25.6	641	bdl	66.1	2.70
BMV	05.18.2017	-1337	37°52'38.1"	16°16'50.1"	13.76	8.10	553	12.6	125	25.3	643	1.38	66.0	2.70
		-1000			13.79	8.09	551	12.6	125	25.5	633	1.04	63.5	2.72
		-500			14.25	8.16	555	12.6	125	25.5	645	1.04	65.8	2.70
		-200			14.88	8.06	555	12.8	126	25.5	643	1.75	65.9	2.66
		-50			15.91	8.07	552	12.7	125	25.5	638	1.09	66.0	2.71
Palizzi PMV	10.06.2003	onland	37°57'51.02"	15°59'28.43"	na	na	15.06	0.09	0.01	0.09	7.23	bdl	3.60	na

Table 1: Chemical composition of the sea water from the studied localities in the Ionian Sea (GeoC1, 2, and 3, and BMV). The chemical composition of the fluids sampled in a well adjacent to the Palizzi mud volcano (PMV) in the Calabria main land is also reported.

Site	depth(m)	He(meq/L)	O$_2$(meq/L)	N$_2$(meq/L)	CH$_4$(meq/L)	CO$_2$(meq/L)	R/Ra	He/Ne
GeoC1	1000	7.14E-05	3.95	9.31	1.37E-04	5.28E-01	0.94	0.30
	900	6.11E-05	3.97	9.64	7.62E-05	5.10E-01	1.07	0.27
	800	7.74E-05	3.75	8.85	7.23E-05	4.73E-01	0.94	0.27
	700	6.86E-05	3.95	9.30	9.14E-05	4.80E-01	1.01	0.24
	500	5.51E-05	4.16	9.45	6.86E-05	4.73E-01	0.93	0.27
	300	5.56E-05	4.10	9.40	8.38E-05	4.95E-01	1.00	0.24
	200	6.35E-05	4.58	9.73	5.61E-05	5.04E-01	0.88	0.27
	100	6.61E-05	4.41	8.90	bdl	4.75E-01	0.93	0.30
GeoC2	1649	6.01E-05	3.93	9.35	2.07E-04	5.64E-01	0.77	0.28
	1500	5.84E-05	4.23	8.98	1.07E-04	5.37E-01	0.92	0.26
	1300	na	3.77	8.98	1.24E-04	4.62E-01	na	na
	1000	na	4.24	9.62	2.30E-05	4.56E-01	na	na
	700	na	4.04	9.99	1.77E-04	4.67E-01	na	na
	600	na	3.94	9.21	6.90E-05	4.39E-01	na	na
	500	na	3.79	8.79	5.82E-05	4.50E-01	na	na
	300	na	4.24	9.48	7.67E-05	4.67E-01	na	na
	100	na	4.38	9.10	1.07E-04	4.54E-01	na	na
GeoC3	2029	8.73E-05	3.98	9.20	5.33E-05	4.54E-01	0.766	0.422
	1500	6.75E-05	3.51	9.85	1.90E-04	4.97E-01	0.950	0.290
	1000	7.17E-05	3.99	9.34	4.57E-05	4.74E-01	0.927	0.366
	500	7.13E-05	3.61	9.33	2.02E-04	4.90E-01	0.976	0.289
	100	na	4.54	9.30	9.14E-05	4.68E-01	na	na
BMV	1337	8.27E-05	3.99	9.12	2.51E-03	7.31E-01	0.73	0.398
	1200	na	3.94	9.33	1.22E-04	5.67E-01	nd	na
	1000	7.70E-05	4.08	9.90	1.45E-04	5.03E-01	0.92	0.256
	800	na	3.97	9.37	9.90E-05	5.22E-01	na	na
	700	na	3.76	8.88	1.07E-04	4.85E-01	na	na
	500	na	3.87	8.60	1.45E-04	4.23E-01	na	na
	300	na	3.97	9.75	1.35E-04	5.50E-01	na	na
	200	na	4.61	9.58	1.52E-04	4.59E-01	na	na
	100	na	6.47	1.59	1.29E-04	4.80E-01	na	na
PMV	onland	2.62E-03	bdl	22.28	6.87E+00	1.23E-01	1.60E-01	17
ASSW		4.80E-05	4.80	9.60	1.00E-06	2.40E-01	1	0.267

Table 2: Dissolved gas composition and helium isotopic ratio of the sea water from the studied localities in the Ionian Sea (GeoC1, 2, and 3, and BMV). Data for the fluids sampled in a well adjacent to the Palizzi mud volcano (PMV) in the Calabria main land are also reported.